9950 - 463

CONCEPTUAL DESIGN STUDY OF CONCENTRATOR ENHANCED SOLAR ARRAYS FOR SPACE APPLICATIONS

Final Report of 2nd Contract Extension Phase 20 October 1980

Subject

Performance Evaluation of 5 KW and 20 KW Systems in Si and GaAs at 1 AU Employing a Flat Plate Trough Concentrator

JPL Contract No. 955194

Hughes Ref No. E3256

HUGHES

HUGHES AIRCRAFT COMPANY
SPACE AND COMMUNICATIONS GROUP
EL SEGUNDO, CALIFORNIA

CONCEPTUAL DESIGN STUDY OF CONCENTRATOR ENHANCED SOLAR ARRAYS FOR SPACE APPLICATIONS

Final Report
of
2nd Contract Extension Phase
20 October 1980

Subject

Performance Evaluation of 5 KW and 20 KW Systems in Si and GaAs at 1 AU Employing a Flat Plate Trough Concentrator

JPL Contract No. 955194

Hughes Ref No. E3256

HUGHES

HUGHES AIRCRAFT COMPANY
SPACE AND COMMUNICATIONS GROUP
EL SEGUNDO, CALIFORNIA

CONCEPTUAL DESIGN STUDY OF CONCENTRATOR ENHANCED SOLAR ARRAYS

FOR

SPACE APPLICATIONS

Final Report of 2nd Contract Extension Phase

20 October 1980

Subject: Performance Evaluation of 5 KW and 20 KW Systems in Si and GaAs at 1 AU Employing a Flat Plate Trough Concentrator

JPL Contract No. 955194
Hughes Ref. No. E3256

Approved: 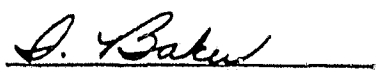

I. Baker
Program Manager
20 October 1980

HUGHES AIRCRAFT COMPANY
Technology Division
Space and Communications Group
El Segundo, California

This work was performed for the Jet Propulsion Laboratory, California Institute of Technology, sponsored by the National Aeronautics and Space Administration under contract NAS-7-100

FINAL REPORT, 2nd CONTRACT EXTENSION

Contents

1.0 INTRODUCTION

The material presented herein constitutes the final report of the second extension to JPL contract no. 955194, "Conceptual Design Study of Concentrator Enchanced Solar Arrays for Space Application". This second extension effort included the conceptualization of a low mass high performance V-trough concentrator and evaluated its performance with both a gallium arsenide and a silicon solar array. The original contract effort was completed and reported upon in May 1979 in a two volume report, Reference 1, while the first contract extension effort was completed and reported upon in March 1980, reference 2.

In the original contract effort, a number of alternative concentrator design concepts were studied for use from 1 to 6 AU. The study, which was limited to silicon solar cell arrays, found that the most effective configurations from among those investigated were the front lit two dimensional flat plate trough concentrator (2D-FPT) for near earth applications or the back lit multiple flat plate concentrator (MFPC) for both near earth and interplanetary missions. When this work was completed, the contract was modified and extended to permit a more comprehensive study of both of these selections. This contract extension effort excluded interplanetary mission considerations and instead was limited to geosynchronous orbit application, but it included gallium arsenide solar arrays as well as silicon. The findings of the extension effort eliminated the MFPC from any further consideration for geosynchronous orbit application.

In the second contract extension effort, the results of which are contained in this report, the objective was to further advance a detailed 2D-FPT design beyond the rough conceptual stage, creating in effect a preliminary design of sufficient maturity to permit more credible mass and performance evaluations.

The following is a more detailed statement of the work that was to be accomplished in this phase of the contract. It has been excerpted from the JPL Statement of Work:

Perform a study to conceptualize a low mass, high performance V-trough concentrator and to evaluate its performance when combined with both a gallium arsenide and a silicon array for use at geosynchronous altitude. The study shall include but not necessarily be limited to the following:

1. Evaluation of the power-to-mass performance of the concentrated array at beginning of life as a function of geometric concentration ratio. The gallium arsenide and silicon arrays shall utilize 18% efficient, 50 micron cells with 75 micron covers and 13% efficient, 50 micron cells with 75 micron covers respectively. A 5 KW and 20 KW concentrated array, beginning-of-life power levels shall be considered. Concentrated silicon array temperature should not exceed +150°C. Concentrated intensity non-uniformity should not exceed 15% for either array.
2. A detailed stress analysis for the representative V-trough structure(s).
3. A thermal analysis with and without the use of advanced cold mirrors.
4. The presentation of a deployment sequence compatible with the shuttle and its launch environment including the stowed configuration and required volumes.
5. Any other pertinent information concerning V-trough performance.
6. Class C drawings.
7. Cost estimates for developmental and flight units.

2.0 SUMMARY AND CONCLUSIONS

A simple, efficient and very light weight preliminary design for a 5 KW and 20 KW BOL output concentrated array has been evolved as a result of this study and is described by the drawings included in the appendix of this report. The relative effectiveness of this design, as compared to an unconcentrated planar array of equal power output, has been measured by comparing power to mass performance of and the solar cell area required by each. As was the case in the concentrator studies of the first contract extension phase, reference 2, the measure of superiority of primary interest was the power to mass performance.

Figures 7.5-1 and 7.5-2 from Section 7.0 (presented again in this section) show the significant results. In this figure, the effort of concentration ratio on the power to mass performance is shown and compared to a planar array of equal output. For the GaAs design, no significant difference in power to mass performance was obtained between the 5 KW and 20 KW output systems. The results were also independent of the type of mirror reflective coating employed. The optimum concentration ratio for the GaAs systems is approximately 3. At this concentration, the power to mass performance is about 42% better than an unconcentrated array of equal power. Note that in every case there is an initial reduction in power to mass as C_g becomes greater than 1. At $C_g = 1$, the power to mass value is based on an unconcentrated array with no mirrors or mirror support structure, although, of course, array blanket deployment and support hardware is included. However, at C_g slightly greater than 1, the power to mass value includes the mirrors and associated structure but the concentration is not yet sufficient to significantly increase the power output. The result is the observed initial dip in the power to mass curve. From the tables in Section 6, it is also shown that array area reductions of 57% are obtainable for GaAs concentrated systems.

The power to mass performance of the concentrated silicon cell arrays is maximum at $C_g = 2$ and is sensitive to both array size and mirror reflective coating. For both array sizes considered, the power to mass values when cold mirror coated reflectors are used are slightly higher, about 5%, than the values with vapor deposited aluminum reflectors. Similarly, the 5 KW systems perform about 15% better in power to mass than do the 20 KW systems because proportionally more massive booms are necessary for the higher power systems. However, no significant improvement in power to mass over the unconcentrated array is shown for any of the concentrated silicon systems, as seen in Fig. 7.5-1. At best, the 5 KW concentrated system employing cold mirror reflectors at the optimum concentration ratio is only 3.5% better than its unconcentrated planar array equivalent. At worst, at the optimum concentration ratio, the

20 KW concentrated system with VDA coated reflectors is inferior by 17% relative to its unconcentrated equivalent. However, in spite of the fact that no improvement in power to mass performance is realizable for silicon systems with the type of concentrator studied, significant reduction in the required number of solar cells is obtained. As determined in Section 6 of this report, about 35% fewer silicon cells are required at the optimum concentration ratio of 2 for any of the concentrated systems as compared to their unconcentrated equivalents.

In summary, it can be stated that by using the type of concentrator studied, improvements in power to mass performance as high as 42% together with array area size reductions of 57% are possible in GaAs systems.

By contrast, when the same concentrator design is applied to silicon systems, no improvement in power to mass can be obtained although array area reductions as high as 35% are obtainable.

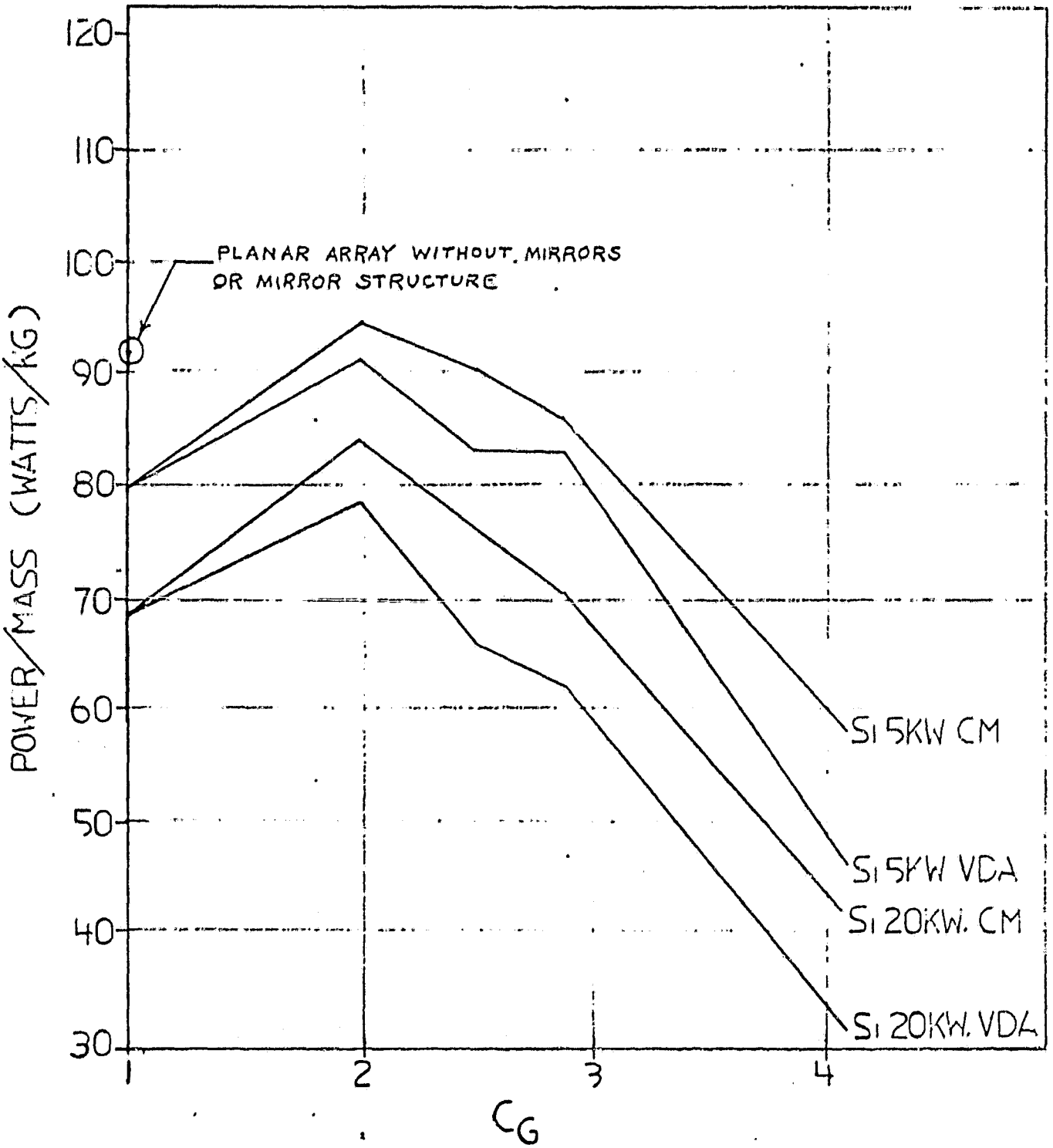

FIGURE 7.5.1

POWER TO MASS PERFORMANCE OF V-TROUGH CONCENTRATED Si ARRAYS

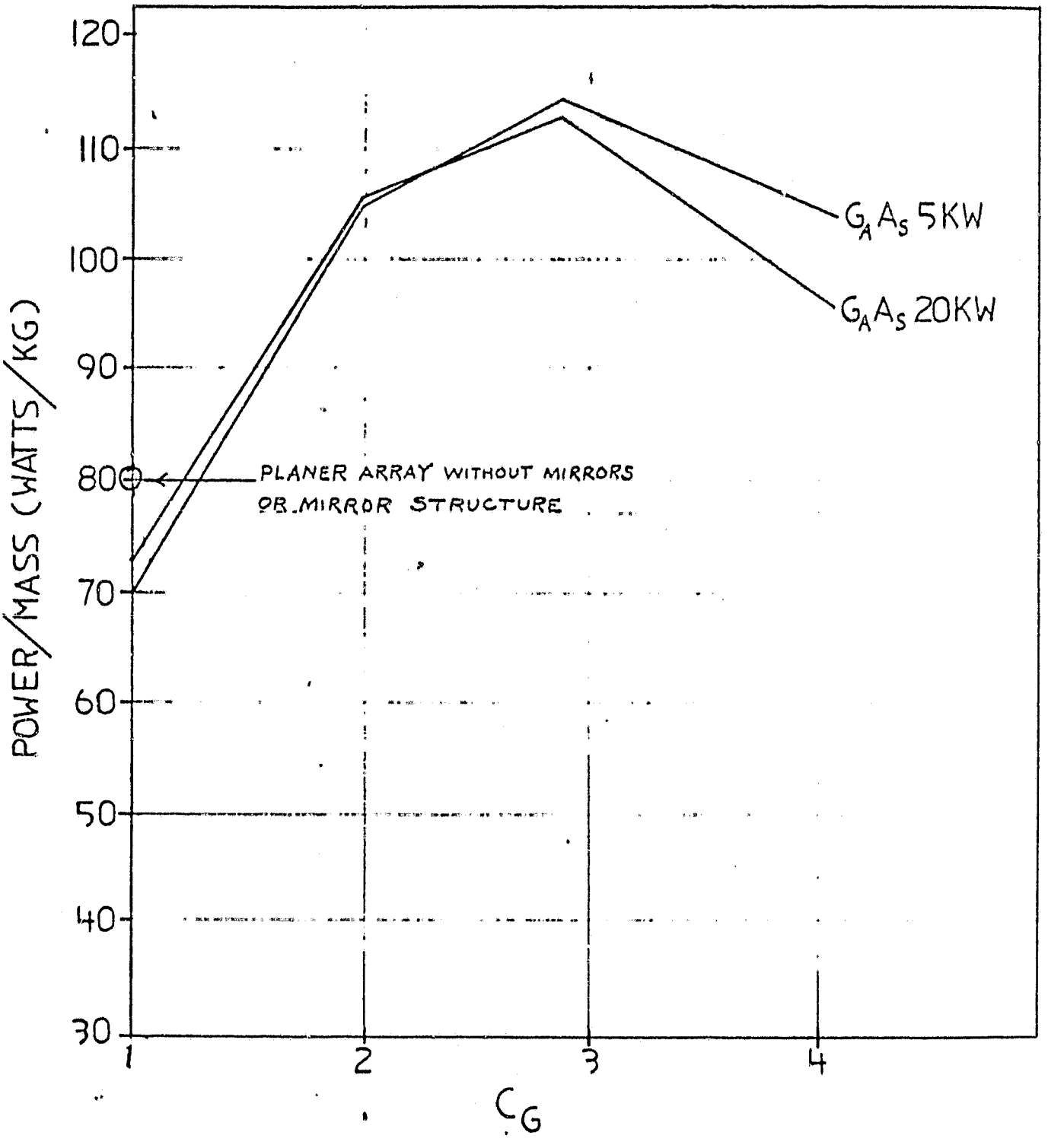

FIGURE 7.5.2

POWER TO MASS PERFORMANCE OF V-TROUGH CONCENTRATED GaAs ARRAYS

3.0 OPTICAL ANALYSIS

In the final report of the first contract extension phase, reference 2, page 11, figure 3.0-2, it was shown that the optimum design to meet the uniformity of illumination requirement with the maximum C_G is design option (1), referred to as the "lost light" design for sun misalignment θ as high as $\theta = \pm 5^\circ$. The figure from reference 2 referred to above, is reproduced here as figure 3.0-0 for the readers convenience. In option (1), the sun misalignment to $\theta = \pm 5^\circ$ is accommodated by oversizing the mirror height. At $\theta = 0^\circ$, incident light on the excess mirror height on both mirrors cannot reach the array and is lost. (Hence, the lost light title). However, as sun misalignment occurs, some of the excess mirror height on one side begins to be effective (reflecting light to the array), while some additional mirror height on the opposite mirror (greater than that which was excess at $\theta = 0^\circ$) becomes ineffective. The mirror oversize height is selected such that when sun misalignment $\theta = 5^\circ$, all the mirror excess height on one mirror becomes totally effective while twice the excess mirror height on the opposite mirror becomes ineffective. As seen in figure 3.0-0, this configuration produces the greatest C_G for all values of θ. A constant portion of incoming light entering the aperture is lost for all values of θ including perfect alignment, $\theta = 0^\circ$, and the light received by the array is completely uniform. The following is a derivation of an equation for the mirror height of this configuration as a function of mirror tilt angle, ϕ, and also an equation for the concentration ratio, C_G, as a function of ϕ. Note that subscripts are used on ℓ and C_G to denote the number of reflections in the configuration being discussed.

The derivation is limited to 1, 2 and 3 reflection cases, but this provides a range of concentration from 1 to 5.

Figure 3.0-1 is a diagram of the concentrator with 2 reflections and no light loss when sun misalignment $\theta = 0$. This corresponds to option (2), Figure 3.0-0. However, as can be seen from this figure, the value of C_G at $\theta = 0$ is the same for options (1) and (2). Therefore, the geometry of Figure 3.0-1 can be used to derive the C_G vs. ϕ equation. In this figure, all dimensions are normalized with respect to the array width. The array width, line bc of figure 3.0-1, is assigned the value of unity, and thus the aperture width, A, is equal to the C_G.

The incoming incident light ray at the left edge of the aperture is normal to the aperture A, line ad. Therefore, the angle that the ray makes with the mirror surface will be $90^\circ - \phi$. The reflected ray will of course make the same angle with the mirror, or angle bae = $90^\circ - \phi$.

Line ej is drawn normal to the mirror at e, intersecting the opposite mirror at f. Line fg is drawn normal to line ej.

Angle f h g = $\emptyset$ the mirror tilt angle

Angle f h g = angle h g f = $\emptyset$

Angle g f h = $180^{\circ} - 2\emptyset$

Angle h f e = $90 - (180^{\circ} - 2\emptyset) = 2\emptyset - 90$

Angle a f e = $180 - (2\emptyset - 90) = 270 - 2\emptyset$

Angle a e f = $180 - (90 - \emptyset) - (270 - 2\emptyset) = 3\emptyset - 180$

Angle a e f = angle f e b (angle of incidence = angle of reflection)

Angle b e c = 90 - angle f e b = $90 - (3\emptyset - 180) = 270 - 3\emptyset$

Angle b c h = $\emptyset$

Angle b c e = $180 - \emptyset$

Angle e b c = $180 - (180 - \emptyset) - (270 - 3\emptyset) = 4\emptyset - 270$

FIGURE 3.0-0

DESIGN OPTIONS AVAILABLE FOR A 2D-FPT CONCENTRATOR AT $\phi = 75°$

(TYPICAL FOR OTHER VALUES OF ϕ)

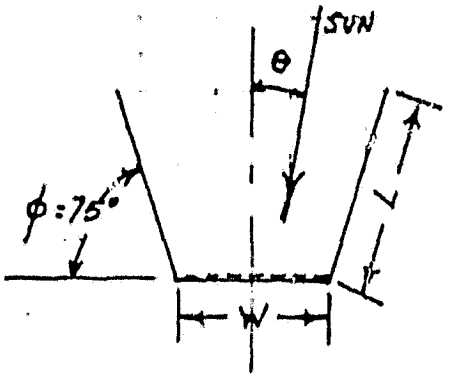

(1) LOST LIGHT DESIGN FOR $\theta = \pm 5°$

Shows max. C_G possible within $\theta = \pm 5°$ allowing lost light at all θ and multiple reflections.

(2) DESIGN FOR NO LIGHT LOSS AT $\theta = 0$ ONLY

Shows max. C_G delivered at any θ to $\pm 5°$ when sized for no light loss at $\theta = 0°$ with multiple reflections. Light loss does occur for all θ other than $\theta = 0°$.

(3) NO LIGHT LOSS DESIGN FOR $\theta = \pm 5°$, MULTIPLE REFLECTIONS

Shows max. C_G possible within $\theta = \pm 5°$. No light loss at any θ and multiple reflections.

(4) NO LIGHT LOSS DESIGN FOR $\theta = \pm 5°$, SINGLE REFLECTION

Same as (3) but limited to one reflection.

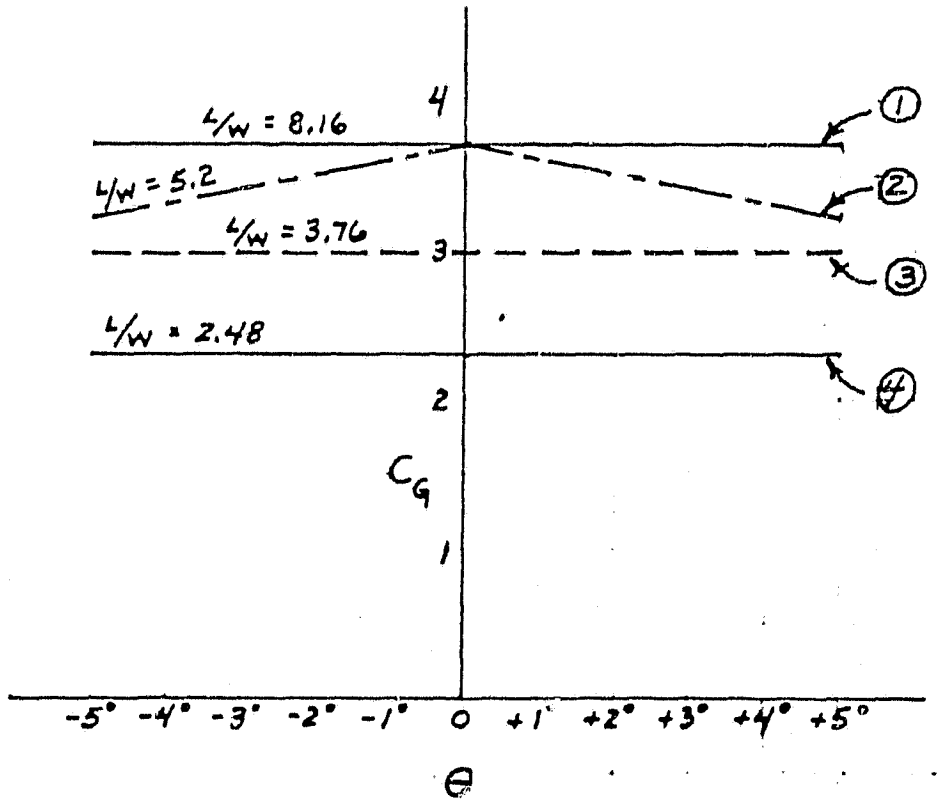

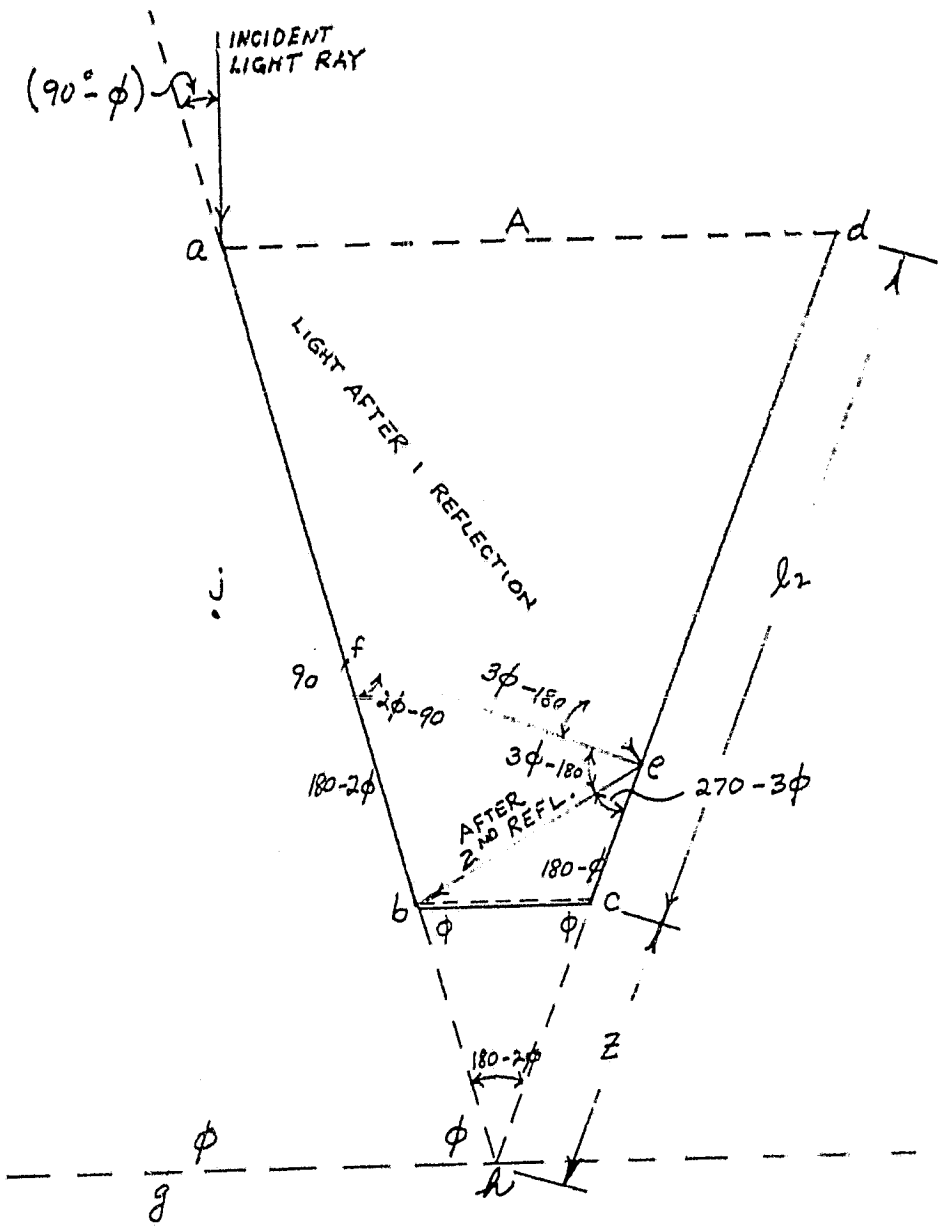

FIGURE 3.0-1 Two Reflection Geometry

$$\frac{\ell_2}{\sin\ (6\emptyset - 360)} = \frac{\text{line b e}}{\sin\ (90 - \emptyset)}$$ (using the law of sines and triangle abe)

$$\ell_2 = \frac{\sin\ (6\emptyset - 360)}{\sin\ (90 - \emptyset)} \cdot (\text{line b e})$$

$$\ell_2 = \frac{\sin 6\emptyset \cos 360 - \cos 6\emptyset \sin 360}{\sin 90 \cos \emptyset - \cos 90 \sin \emptyset} \cdot \text{line b e}$$

$$\ell_2 = \frac{(\sin 6\emptyset)}{(\cos \emptyset)} \cdot \text{line b e}$$

but line b e $= \frac{\sin\ (180 - \emptyset)}{\sin\ (270 - 3\emptyset)} = \frac{\sin 180 \cos \emptyset - \cos 180 \sin \emptyset}{\sin 270 \cos 3\emptyset - \cos 270 \sin 3\emptyset}$

$= -\frac{\sin \emptyset}{\cos 3\emptyset}$ (from law of sines and triangle bce, noting that line bc = 1)

$$\ell_2 = -\frac{\sin 6\emptyset}{\cos \emptyset} \cdot \frac{\sin \emptyset}{\cos 3\emptyset}$$

NOTE: This equation is not to be used for the lost light configuration (1) because it does not include an oversi for sun misalignment θ.

Let Z = line b h

$$Z = \frac{\frac{1}{2}}{\cos \emptyset} = \frac{1}{2 \cos \emptyset}$$

$$\frac{A}{\ell_2 + Z} = \frac{1}{Z}$$ (note that line ad = A and line bc = 1)

$$A = \frac{\ell_2 + Z}{Z} = \frac{\ell_2}{Z} + 1$$

$$A = 1 - \frac{\sin 6\emptyset}{\cos \emptyset} \cdot \frac{\sin \emptyset}{\cos 3\emptyset} \cdot 2 \cos \emptyset = C_{G_2}$$

$$C_{G_2} = 1 - \frac{2 \sin 6\emptyset \sin \emptyset}{\cos 3\emptyset}$$ (2 REFLECTION CASE) ---------- (1)

This result can be used for either the lost light conf. (1) or θ = 0 no light loss conf. (2).

The subscript no. 2 signifies that this result is only valid for the 2 reflection case. Note that two reflections are only possible as long as each ray after second reflection makes an angle with the solar array that is greater than 0., i.e., angle e b c is $>$ 0. Since angle e b c = $4\phi - 270$

$\phi > 67.50^{\circ}$ to achieve 2 reflections

Obviously, if $\phi < 67.5^{\circ}$, only 1 reflection is possible. To solve for the required mirror height ℓ_2 for the 2 reflection case, lost light configuration (1), (see figure 3.0-0) it is only necessary to assume a $\theta = 5^{\circ}$ sun angle misalignment in the original incident light ray of Figure 3.0-1. Thus the angle between the mirror and the incoming light ray is $90^{\circ} - \phi - 5^{\circ}$ or $85^{\circ} - \phi$. By working through the same geometry as before, the equation for ℓ_2 can be obtained.

Angle b a e = $85^{\circ} - \phi$

Angle a f e = $270 - 2\phi$ as before

Angle a e f = $180 - (85 - \phi) - (270 - 2\phi) = 3\phi - 175$

Angle f e b = a e f = $3\phi - 175$

Angle b e c = $90 - (3\phi - 175) = 265 - 3\phi$

Angle e b c = $180 - (180 - \phi) - [90 - (3\phi - 175)] = 4\phi - 265$

$$\frac{\text{line b e}}{\sin (180 - \phi)} = \frac{1}{\sin (265 - 3\phi)}$$

$$\text{line b e} = \frac{\sin (180 - \phi)}{\sin (265 - 3\phi)}$$

$$\frac{\ell_2}{\sin (6\phi - 350)} = \frac{\text{line b e}}{\sin (85^{\circ} - \phi)}$$

$$\ell_2 = \frac{\sin (6\phi - 350)}{\sin (85 - \phi)} \cdot \frac{\sin (180 - \phi)}{\sin (265 - 3\phi)} \qquad (67.5 < \phi) \ldots\ldots\ldots\ldots (2)$$

Equation (1) can be used for C_{G_2} and equation (2) for ℓ_2 within the range of ϕ for which 2 reflections will occur. As derived previously, the lower limit of the 2 reflection range is $\phi = 67.5^{\circ}$. Below 67.5° only one reflection will occur. Therefore, 67.5° is also the upper limit of the one reflection range. To obtain the upper limit of the 2 reflection range, it is necessary to study the geometry of the 3 reflection case and determine the lower limit of its range. This would then be

the upper limit of the 2 reflection case. Figure 3.0-2 shows the geometry for 3 reflections. As before, the aperture width for this case is derived by setting the sun misalignment angle θ equal to zero. This aperture width will be equal to the C_{G_3}. The values of the pertinent angles are obtained by geometry and by the law of reflection as before and are shown in the figure. In a manner similar to that previously described, the equation for C_{G_3} was derived.

$$C_{G_3} = 1 + \frac{2}{\sin(90-5\phi)} \cdot \left[\sin(90-\phi)\sin(6\phi-90) + \frac{\sin 6\phi \sin(270-7\phi)\sin(180-\phi)}{\sin(270-3\phi)} \right]$$

similarly, by including the sun misalignment angle θ in the geometry, the equation for ℓ_3 was derived.

$$\ell_3 = \left[\frac{\sin(6\phi-90+\theta)}{\sin(90-5\phi-\theta)} + \frac{\sin(6\phi+2\theta)\sin(270-7\phi-\theta)\sin(180-\phi)}{\sin(90-\phi-\theta)\sin(270-3\phi-\theta)\sin(90-5\phi-\theta)} \right]$$

From Figure 3.0-2 it can be seen that the lower limit of the ϕ range for 3 reflections (which is the upper limit for 2 reflections) occurs when $6\phi-90 \geq 0$.

$$\therefore \quad 6\phi \geq 90$$

$$\phi \geq \frac{90}{6}$$

$$\phi \geq 15, \text{ or } 75, \text{ or } 135$$

However, the concentrator can only operate when

$$(45 \leq \phi \leq 90)$$

Therefore the solution is $\phi \geq 75^{\circ}$.

Figure 3.0-3 shows the geometry for 1 reflection. From this geometry

$$C_{G_1} = 2 \sin(2\phi - 90) + 1$$

$$\ell_1 = \frac{\sin(2\phi - 90 + \theta)}{\sin(90 - \phi - \theta)}$$

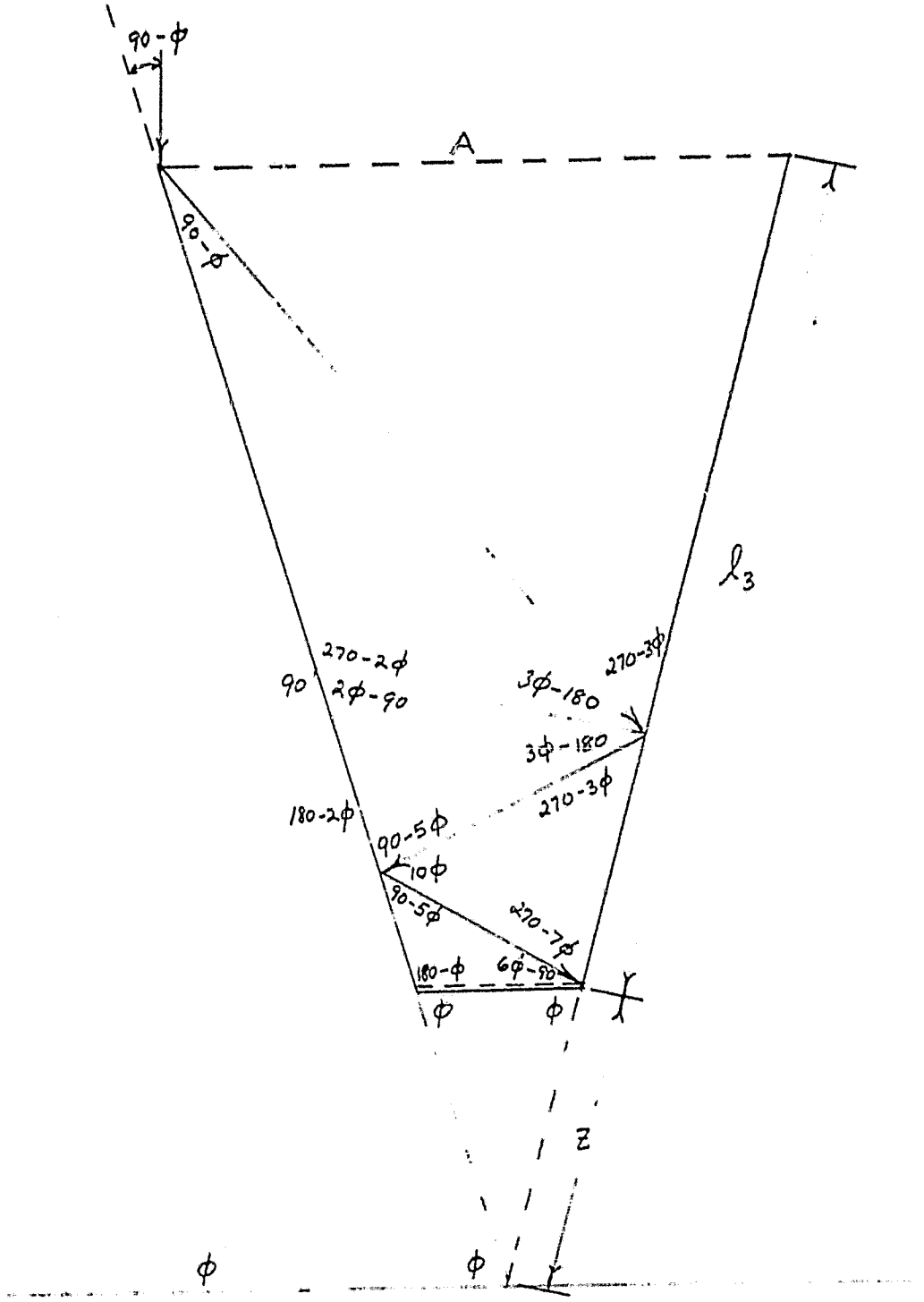

FIGURE 3.0-2 Three Reflection Geometry

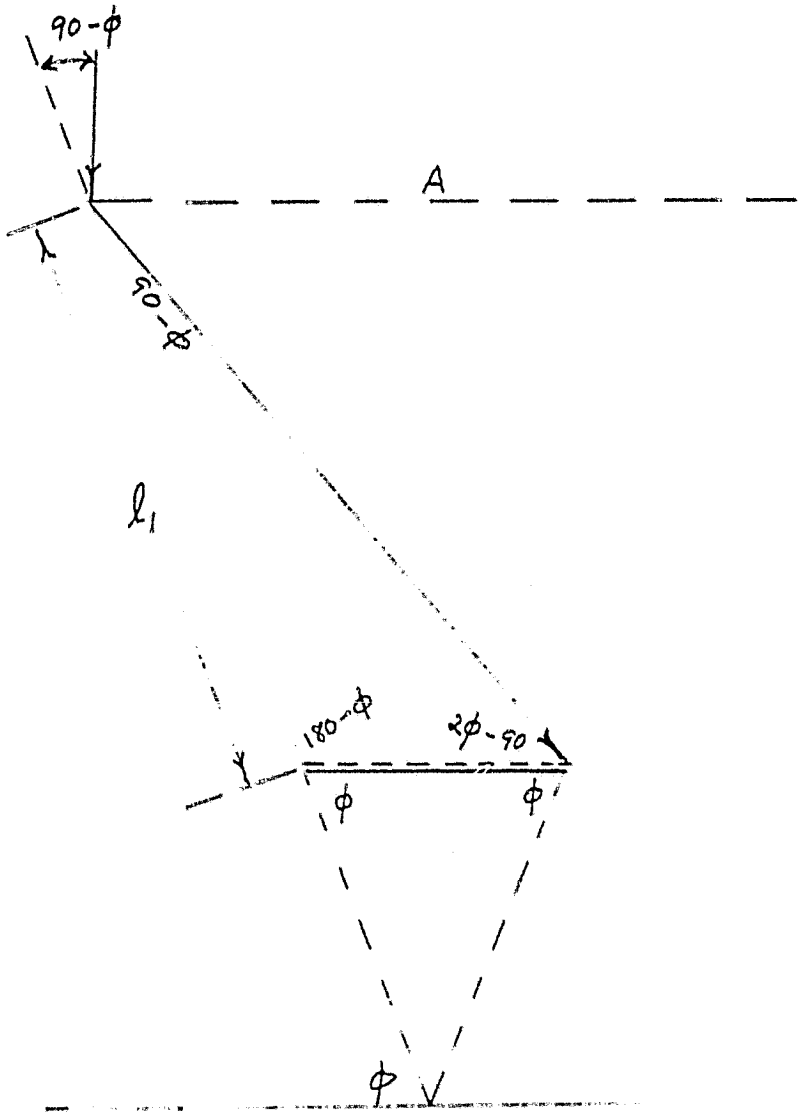

FIGURE 3.0-3 One Reflection Geometry

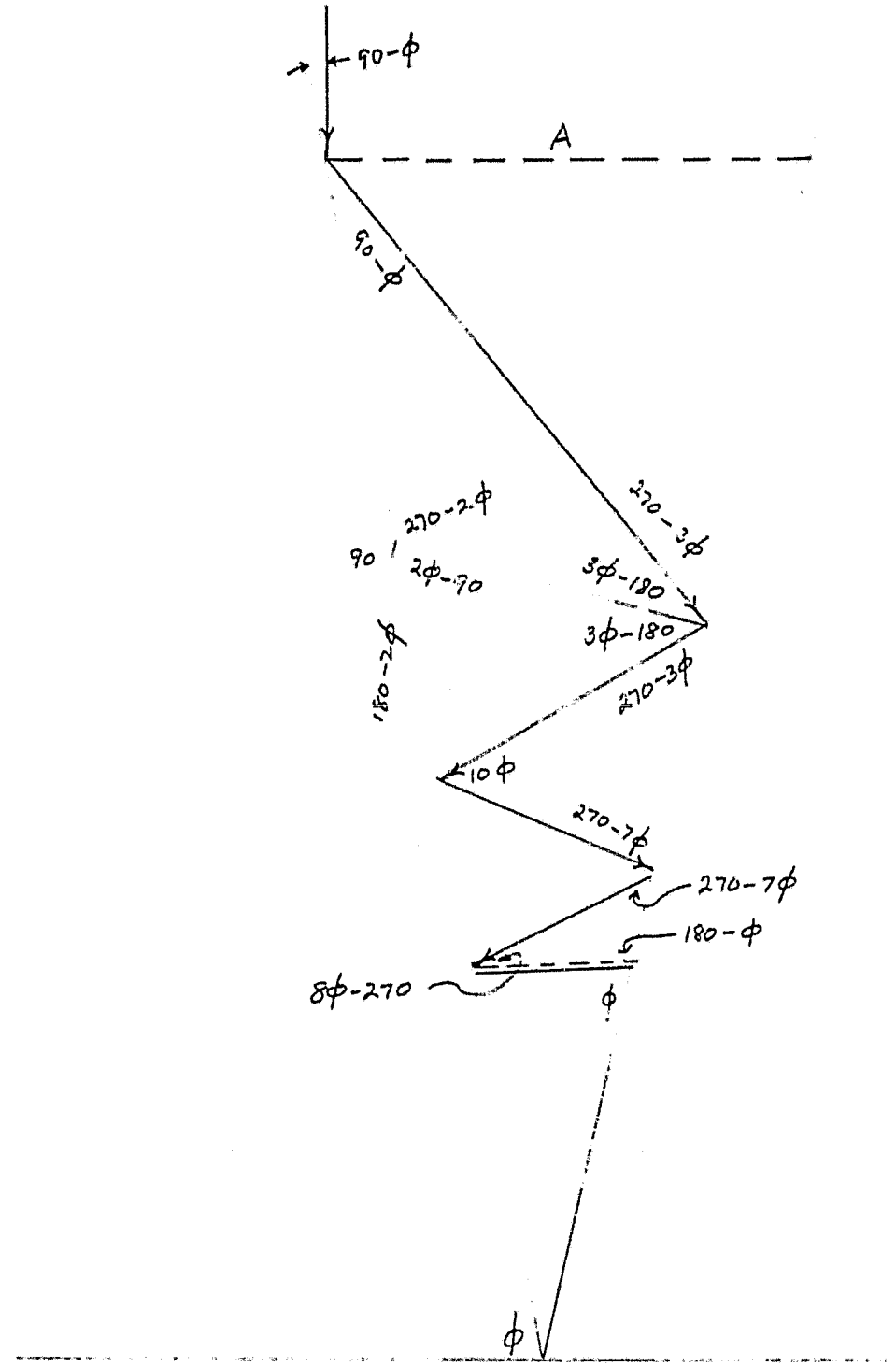

FIGURE 3,0-4 Four Reflection Geometry

The lower limit of ϕ for 1 reflection is given by

$$2\phi - 90 \geq 0$$
$$2\phi \geq 90$$
$$\phi \geq 45^{\circ}$$

The upper limit of the range of ϕ for the 3 reflection case is obtained as the lower limit of the ϕ range for the 4 reflection case. Figure 3.0-4 shows the 4 reflection geometry. Again, as in the previous geometries, 4 reflections can only occur if the angle that the 4th reflected ray makes with the solar array is greater than or equal to zero. Hence

$$8\phi - 270 \geq 0$$
$$8\phi \geq 270 \text{ or } 630 \text{ or } 990, \text{ etc.}$$
$$\phi \geq 33.75 \text{ or } 78.75 \text{ or } 123.75$$

but only 78.75 has practical meaning since

$$45 < \phi < 90 \text{ for concentrator operation.}$$

$$\therefore \phi \geq 78.75$$

Now using the derived equations for C_{G_1}, C_{G_2}, and C_{G_3} and for $\ell_1, \ell_2,$ and ℓ_3, together with the ranges for ϕ over which these equations are applicable, a table of concentration ratio and mirror height versus mirror tilt angle was constructed. The results are shown as Table 3.0-1

TABLE 3.0-1 MIRROR HEIGHT AND CONCENTRATION RATIO AS A FUNCTION OF MIRROR TILT ANGLE (UNIT ARRAY WIDTH) $-5^{\circ} \leq \theta \leq 5^{\circ}$

ϕ (Deg.)	No. of Reflections N	C_G	ℓ_N
45	1	1.00	--
50	1	1.35	.45
55	1	1.68	.84
60	1	2.00	1.36
65	1	2.28	2.07
67.5	1	2.41	2.55
68	2	2.51	3.07
70	2	2.88	4.16
75	2	3.73	8.52
76	3	4.093	11.13
77	3	4.445	13.71
78.75	3	5.027	20.04

4.0 THERMAL ANALYSIS

The thermal analysis task during the second contract extension period included the following:

- o Extension of the 2D-FPT concentrator (Lockheed V-trough) analysis reported in Reference 2 to an array design utilizing advanced (low thermal energy absorptance) GaAs or silicon solar cells.
- o Prediction of unconcentrated array temperatures utilizing these same cells.

The array temperature predictions for the 2D-FPT concentrator design are shown in Figures 4.0-1 and 4.0-2 for VDA and cold mirror reflector finishes, respectively. These results were obtained using the computational methods described in Reference 2. The environment assumed was for a geosynchronous orbit at winter solstice with no allowance for cell radiation degradation or thermal inputs from other spacecraft elements. The solar cell absorptances are based upon projected improvements in future cell design utilizing front surface UV reflective coatings and back surface coatings to reflect infrared energy. Figure 4.0-3 illustrates the assumed modification to the GaAs spectral reflectance required to achieve the solar absorptance of 0.58. The unmodified data shown are those presented in Reference 2. Similar assumptions were made for the silicon cell. Cell efficiencies, accounted for in the array heat balance, were taken from the data presented in Section 5.0.

The cold mirror spectral properties assumed in this analysis are those cited in Reference 2 for an OCLI coating. The array aft side emittance was assumed to be .65, consistent with bare 1 mil Kapton. The effects on array temperatures of assuming a 0.85 emittance are shown in Figures 4.0-4 and 4.0-5. This emittance could be achieved in the design by applying a thermal paint (several mils thick, hence adding significant weight) or by carbon impregnation of the Kapton. The latter approach requires materials development, the extent of which was not investigated in this study.

Table 4.0-1 presents predicted array temperatures for unconcentrated designs based on the same parameters used in the 2D-FPT analysis. Additional data are shown for summer solstice and equinox seasons as well as for solar absorptance (α) consistent with currently utilized solar cells.

Figure 4.0-1
Solar Array Temperatures with 2D-FPC Concentrator

VDA Reflector Finish ($\rho = .9$)

Concentrator Distortion Loss = .1

Concentrator Oversized for ±5° Sun Misalignment

Geosynchronous Orbit

Winter Solstice

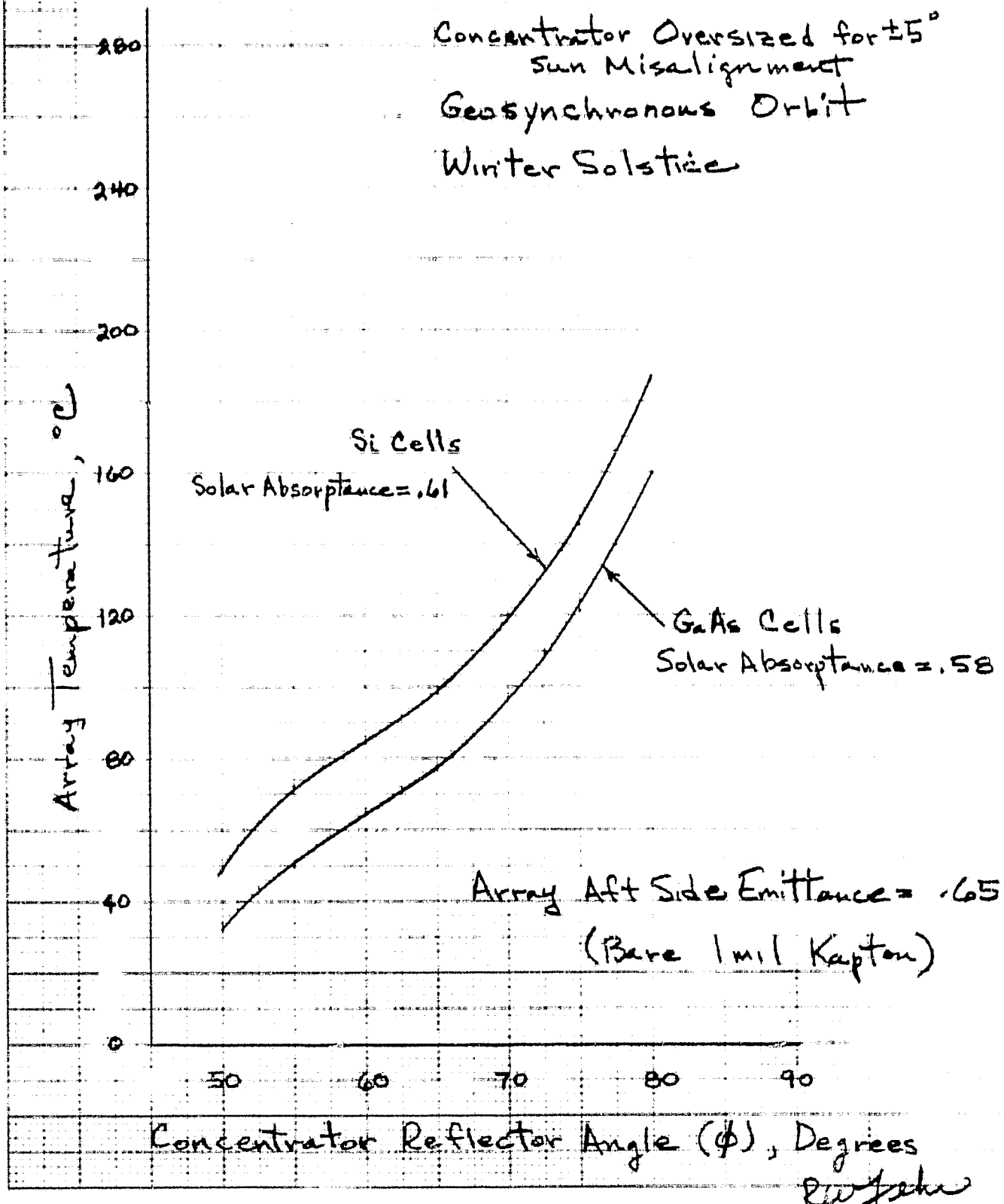

R. Wolfe
9/15/60

Figure 4.0-2
Solar Array Temperatures with 2D-FPC Concentrator

Cold Mirror Reflector Finish ($\rho = .50$)
Concentrator Distortion Loss = .1
Concentrator Over-sized for ± 5° Solar Misalignment
Geosynchronous Orbit

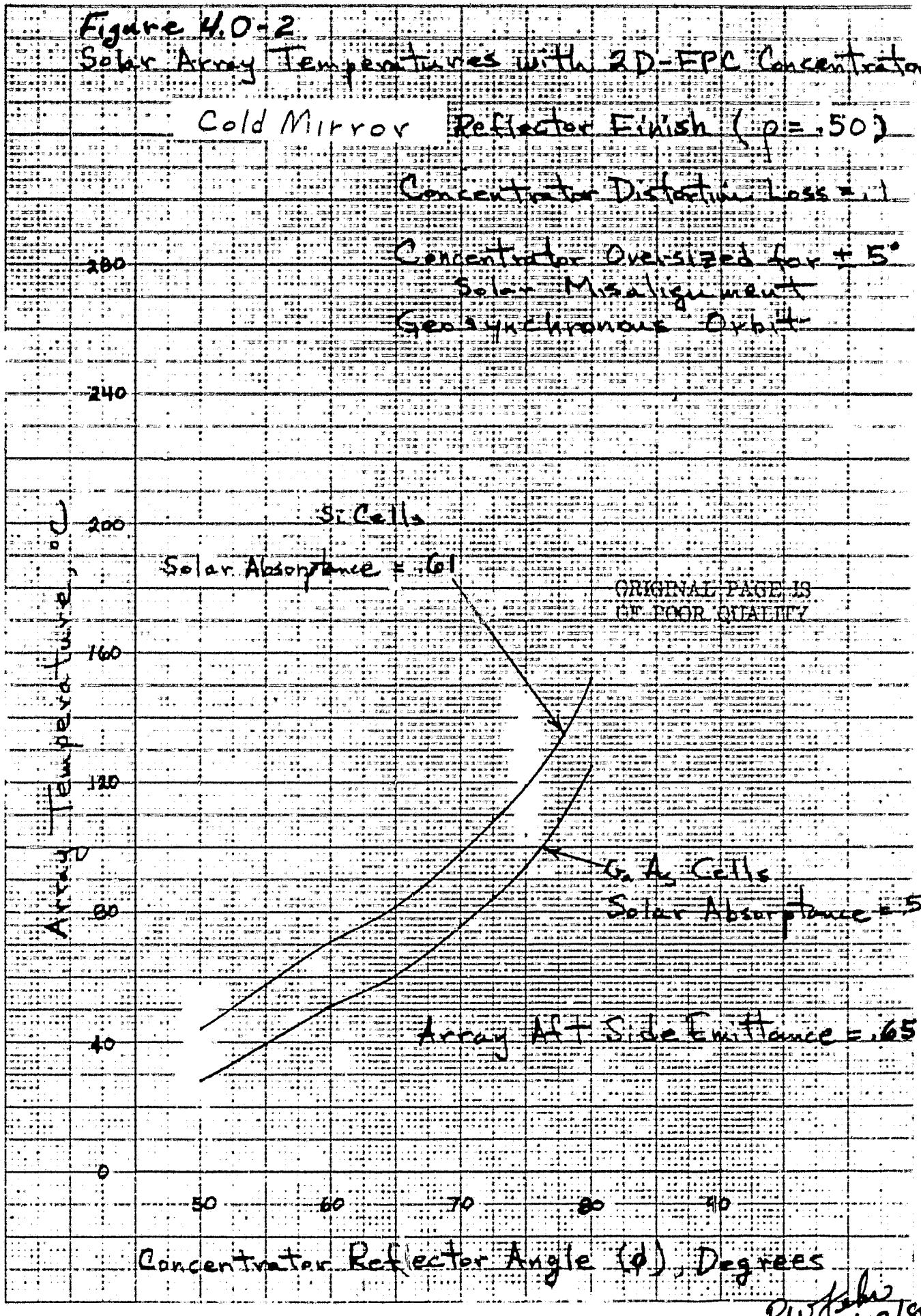

RW Fahrig 9/22/80

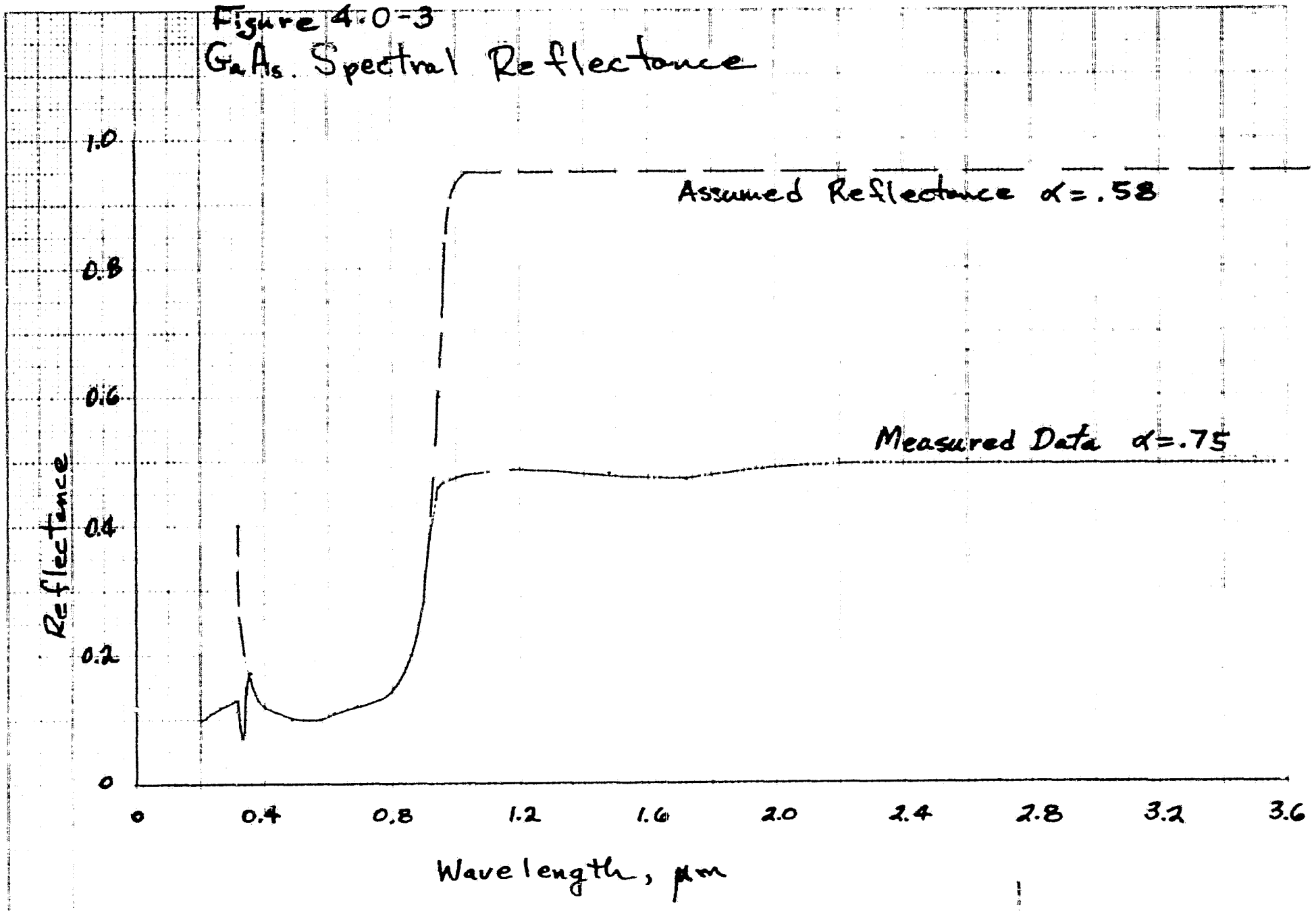
Figure 4.0-3
GaAs. Spectral Reflectance
Assumed Reflectance α=.58
Measured Data α=.75
Reflectance
1.0
0.8
0.6
0.4
0.2
0
0
0.4
0.8
1.2
1.6
2.0
2.4
2.8
3.2
3.6
Wavelength, μm

Figure 4.0-4

Solar Array Temperatures with 2D-TPC Concentrator

VDA Reflector Finish ($\rho = .9$)

Concentrator Distortion Loss = .1

Concentrator Oversized for ± 5° Solar Misalignment

Geo-synchronous Orbit

Winter Solstice

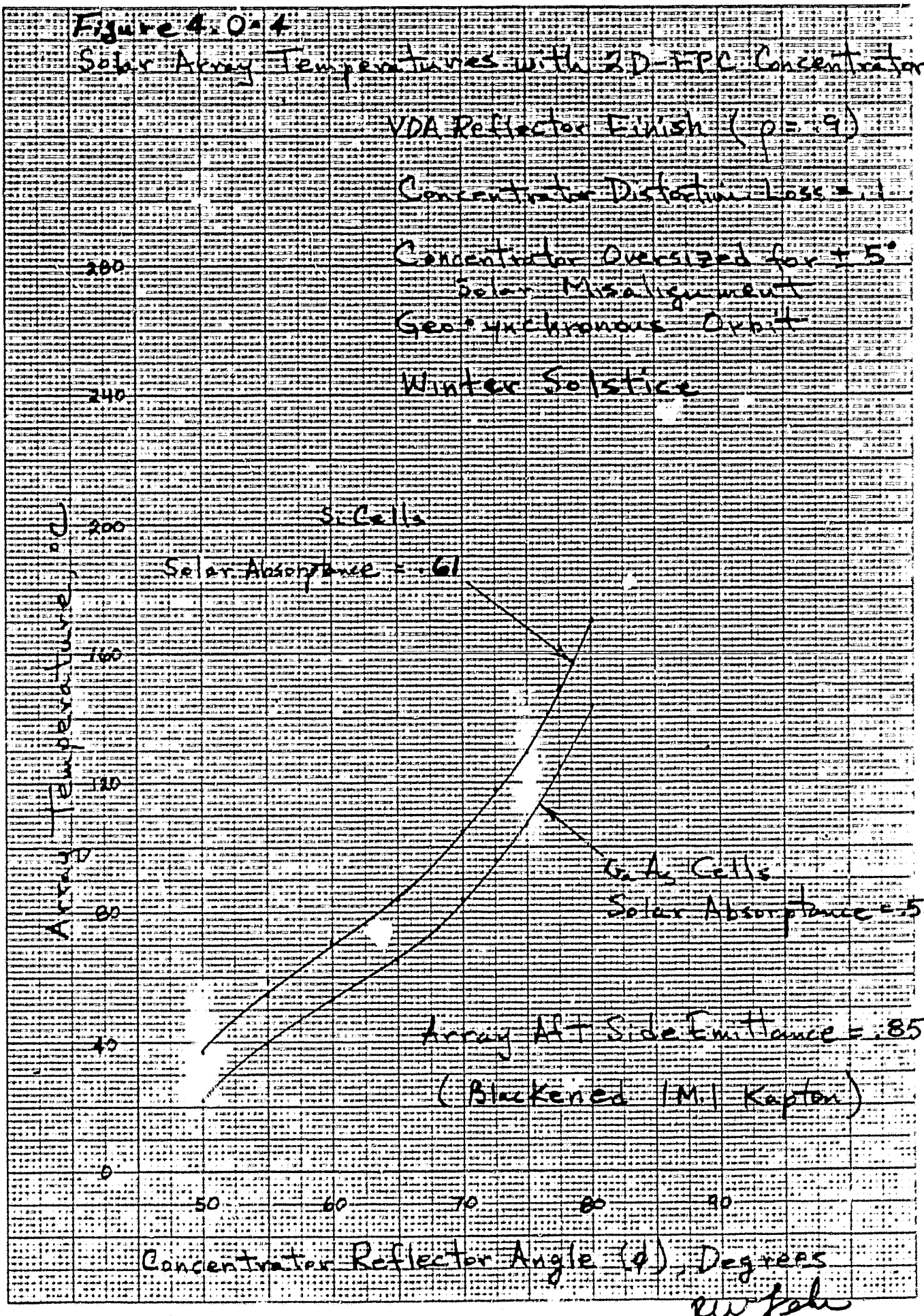

R.W. Forbes
9/15/80

Figure 4.0-5

Solar Array Temperatures with 2D-FPC Concentrator

Cold Mirror Reflector Finish ($\rho = .50$)

Concentrator Distortion Loss = .1

Concentrator Oversized for ± 5° Solar Misalignment

Geosynchronous Orbit

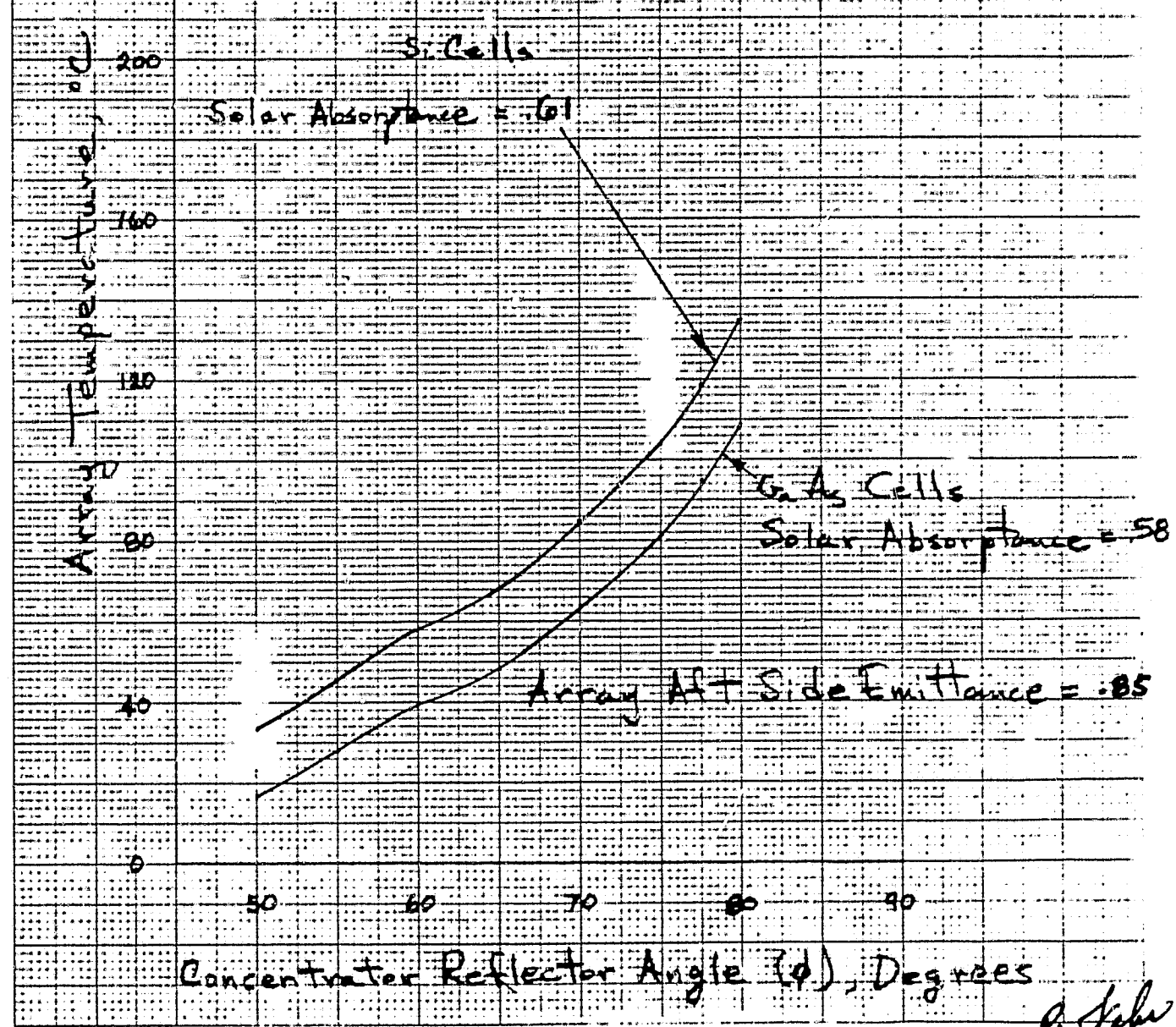

R.W. Fabel 9/22/80

TABLE 4.0-1

UNCONCENTRATED SOLAR ARRAY TEMPERATURES

GEOSYNCHRONOUS ORBIT

NO RADIATION DEGRADATION ASSUMED

CELL TYPE	ARRAY TEMPERATURE, °C					
	BARE KAPTON BACKSIDE FINISH			BLACKENED BACKSIDE FINISH		
	Summer Solstice	Equinox	Winter Solstice	Summer Solstice	Equinox	Winter Solstice
Si α = .84	54	57	60	43	46	48
η = .61	21	24	26	11	13	16
GaAs η = .751	36	38	40	25	27	30
η = .58	8	10	12	-2	0	2

ASSUMED SOLAR INTENSITY:

Summer Solstice = 131.5 mW/cm^2

Equinox = 135.3 mW/cm^2

Winter Solstice = 139.4 mW/cm^2

Forward Side Emittance = .8

BACKSIDE SURFACE EMITTANCE:

1 mil Kapton = .65

Blackened Kapton = .85
(Painted, Carbon impregnated)

5.0 SOLAR CELL PROPERTIES SELECTION

The Statement of Work for the second contract extension phase of the program specified that the silicon solar cells used in the solar array for this design study be 50 microns thick, incorporate a 75 micron cover and be 13% efficient at BOL. Similarly, the Statement of Work also specified the same thicknesses of cell and cover for the Gallium Arsenide cells but called in that case for a 18% BOL efficiency. To ultimately evaluate power to mass characteristics of the designs studied, it was necessary to further select in relatively complete detail all the other elements and characteristics that would make up the complete solar blanket for each of these cells. The selection of these details was accomplished by exercising the judgement of the company's solar cell specialists by having them list what they believed could be currently accomplished for a minimum weight maximum performance blanket with state-of-the-art. The selection of details so obtained was then discussed with the customer (JPL) until a mutually agreed upon breakdown was established. Tables 5.0-1 and 5.0-2, for a 100V silicon cell array and a 100V gallium arsenide cell array respectively, show the selected details. In each table, for contrast, selections were made based on current 1980 technology, near future technology and advanced development predictions. In both tables, however, only the current 1980 technology selections were actually utilized in the design study. Table 5.0-3 (which provides a direct comparison between the selected silicon details and the gallium arsenide details for the same time frame and conditions,) is also presented for convenience. Note also that on the bottom of this table, power to mass performance of the blankets are shown. These figures assume the blanket is in geosynchronous orbit, but do not account for the additional structure that would be required to package, deploy and support it. Actual figures for an unconcentrated flight array rather than just a blanket would, therefore, be considerably lower.

The effect of temperature on the efficiency of the selected 1980 technology cells is shown in Figure 5.0-1. The data represents Hughes best judgement, at the time of this report, as to the most appropriate values to use from test data available from multiple sources. The effect of increased solar intensity due to concentration is considered second order and was ignored.

TABLE 5.0-1 – SELECTED Si SOLAR CELL BLANKET CHARACTERISTICS

SILICON N/P	1980 TECHNOLOGY - 100V BUS						NEAR FUTURE - 175V BUS						ADVANCED DEVELOPMENT - 175V BUS					
	PACK FACTOR PERCENT	THICK MICRO-METERS	TYPE MATL	DENSITY G/CC	MASS MG/CM^2	PERCENT TOTAL	PACK FACTOR PERCENT	THICK MICRO-METERS	TYPE MATL	DENSITY G/CC	MASS MG/CM^2	PERCENT TOTAL	PACK FACTOR PERCENT	THICK MICRO-METERS	TYPE MATL	DENSITY G/CC	MASS MG/CM^2	PERCENT TOTAL
COVER	90	75	CSM	2.6	(17.6)	(23.5)	90	50	CSX	2.5	(11.3)	(27.3)	100	25	CLEAR POLYMIDE	1.7	(4.25)	
COVER ADH	90	62	SILI-CONE	1.1	(6.1)	(9.1)	25% FRAME	25	FEP	2.16	(4.9)	(11.9)		0	(PART OF COVER)			
COVER ASSY					23.7	32.6					16.2	41.9					4.25	17.87
FRONT CONTACT		3-5	Ag	10.4	(0.3)	(0.4)		3-5	Ag	10.4	(0.3)	(0.7)		3-5	Ag	10.4	(0.3)	
CELL		62	Si	2.4	(14.9)	(19.9)		62	Si	2.4	(14.9)	(35.6)		50	Si	2.4	(12.0)	
BSF			No		-	-			BORON		NEG	-			BORON		-	
GLUE METAL			Ti		NEG	-			Cr		NEG	-			Cr			
BSR		1	Al	2.7	NEG	-		1	Cr	7.2	NEG	-		1	Cr	7.2	NEG	
REAR CONTACT	FULL	3-5	Ag	10.4	(4.2)	(5.6)	GRID	3-5	10.4	7.2	(0.3)	(0.7)	GRID	3-5	10.4	4.2	(0.3)	
CELL ASSY					19.4	25.9					15.5	40.1					12.6	53.0
INTERCONNECT		25	Ag	10.4	15	20		12.5	Al	2.8	0.8	7.1		12.5	Al	2.8	0.8	3.35
CELL ADH	82	40	RTV GLASS FABRIC	1.3	6.3	8.4	90	20	RTV	1.1	2.4	6.2	90	20	RTV	1.1	2.4	10.03
SUBSTRATE	82	25	KAPTON	1.44	4.4	5.9	90	12.5	GLASS REINF. KAPTON	1.44	2.0	5.2	90	12.5	GLASS REINF. KAPTON	1.44	2.0	8.41
BUS STRIPS		25	Cu	8.94	5.3	7.1		25	Cu	8.94	1.73	4.5		25	Cu	8.94	1.73	7.28
TOTAL					74.1						38.63						23.78	

8/22/2c
FSD

TABLE 5.0-2 – SELECTED GaAs SOLAR CELL BLANKET CHARACTERISTICS

GaAlAs P/N	1980 TECHNOLOGY – 100 V BUS						NEAR FUTURE – 175 V BUS						ADVANCED DEVELOPMENT – 175 V BUS					
	PACK FACTOR PERCENT	THICK MICRO-METERS	TYPE MATL	DENSITY G/CC	MASS MG/CM^2	PERCENT TOTAL	PACK FACTOR PERCENT	THICK MICRO-METERS	TYPE MATL	DENSITY G/CC	MASS KG/CM^2	PERCENT TOTAL	PACK FACTOR PERCENT	THICK MICRO-METERS	TYPE MATL	DENSITY G/CC	MASS MG/CM^2	PERCENT TOTAL
COVER	90	75	CSM	2.6	(17.6)		90	50	CSX	2.5	(11.3)		100	25	CLEAR POLYMIDE	1.7	(4.25)	
COVER ADH	90	62	SILI-CONE	1.1	(6.1)		25% FRAME	25	FEP	2.16	(4.9)			0	(PART OF COVER)			
COVER ASSY					23.7	14.9					16.2	31.9					4.25	20.83
FRONT CONTACT		3	Ag	10.4	(0.3)			3	Ag	10.4	(0.3)			3	Au	10.4	(0.3)	
CELL		200	GaAs	5.3	(106)			50	GaAs	5.3	(27)			5	GaAs	5.3	(2.7)	
BSF			–						–						–			
GLUE METAL			Au		NEG				Au	NEG					Au		NEG	
BSR																		
REAR CONTACT		2	Ag	10.4	(2)		GRID	3	Ag	104	(0.3)			2	Al	2.8	(0.56)	
CELL ASSY					108.3	66.2					27.6	54.4					3.56	24.15
INTERCONNECT		25	Ag	10.4	15	9.2		12.5	Al	2.8	0.8	1.6		12.5	Al	2.8	0.8	5.43
CELL ADH	82	40	RTV GLASS FABRIC	1.3	6.3	3.8	90	20	RTV	1.1	2.4	4.7	90	20	RTV	1.1	2.4	16.28
SUBSTRATE	82	25	KAPTON	1.44	4.4	2.7	90	12.5	GLASS REINF. KAPTON	1.44	2.0	3.9	90	12.5	GLASS REINF. KAPTON	1.44	2.0	13.57
BUS STRIPS		25	Cu	8.94	5.3	3.2		25	Cu	8.94	1.73	3.4		25	Cu	8.94	1.73	11.74
TOTAL					163.0						50.73						14.74	

8/22/80

TABLE 5.0-3 COMPARISON OF SELECTED Si AND GaAs SOLAR CELL BLANKET CHARACTERISTICS

	1980 Si		1980 GaAlAs		NEAR FUTURE Si		NEAR FUTURE GaAlAs		ADV. DEV. Si		ADV. DEV. GaAlAs	
	MG/CM^2	PERCENT TOTAL	MG/CM^2	PERCENT TOTAL	MG/CM^2	PERCENT TOTAL	MG/CM^2	PERCENT TOTAL	MG/CM^2	PERCENT TOTAL	MG/CM^2	PERCENT TOTAL
COVER ASSY	23.7	32.6	23.7	14.9	16.2	41.9	16.2	31.9	4.25	17.87	4.25	28.83
CELL ASSY	19.4	25.9	108.3	66.2	15.5	40.1	27.6	54.4	12.6	53.0	3.56	24.15
INTERCONNECT	15	20	15	9.2	0.8	2.1	0.8	1.6	0.8	3.36	0.8	5.43
CELL ADH	6.3	8.4	6.3	3.8	2.4	6.2	2.4	4.7	2.4	10.1	2.4	16.28
SUBSTRATE	4.4	5.9	4.4	2.7	2.0	5.2	2.0	3.9	2.0	8.4	2.0	13.57
BUS STRIPS	5.3	7.1	5.3	3.2	1.73	4.5	1.73	3.4	1.73	7.28	1.73	11.74
TOTAL	74.1	100	163.0	100	38.63	100	50.73	100	23.78	100	14.74	100

PERFORMANCE W/KG										
	1)	166	121	383	414	558	1424
	2)	176	124	406	423	592	1454

1) BARE KAPTON BACK SURFACE

2) BLACK KAPTON BACK SURFACE

PSD
8/22/80

FIGURE 5.0-1 Cell Efficiency Vs Temperature

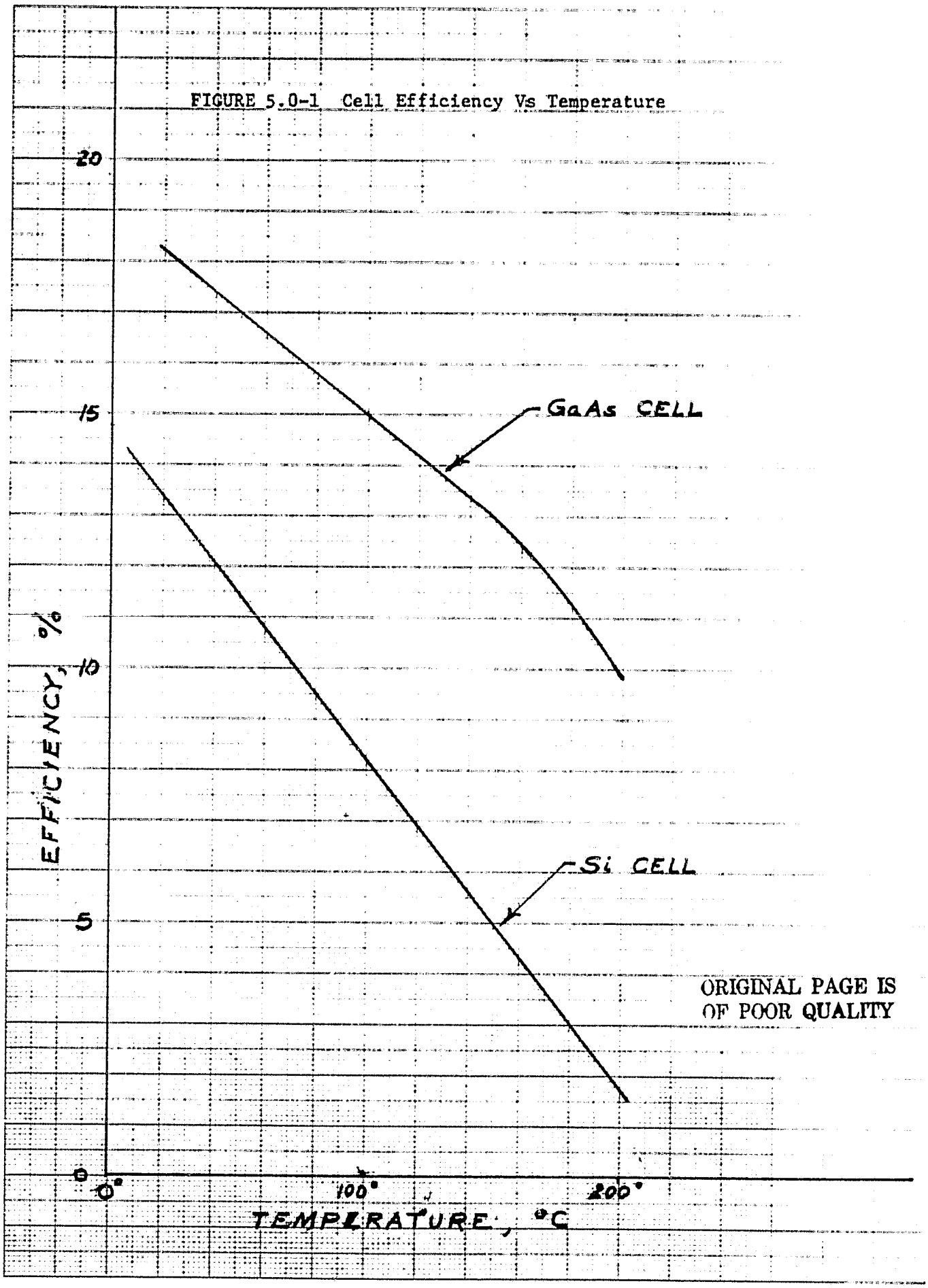

6.0 SYSTEM EVALUATION

The objective of this task is to determine the array area required to generate the required total power for each value of mirror tilt angle, hence concentration ratio, considered. All calculations were carried out for GaAs and then repeated for Si solar cells.

As a starting point, the power output characteristics of the unconcentrated solar array in geosynchronous orbit, assuming 55°C ambient temperature was calculated.

6.1 Gallium Arsenide Arrays

At 55°C winter solstice, Efficiency, N_o = 16.6%

Power Output P_o = Solar Constant x N_o x losses

$$P_o = 135.3 \times 1.03 \times .166 \times .90 \times .97 \times .96 \times .995 \ \frac{mW}{Cm^2}$$

The factor 1.03 accounts for the increased solar energy that occurs during winter solstice (all temperature calculations were made for this season, see Section 4.0). The losses .90, .97, .96 and .995 are a packing factor, assembly loss, bussing loss and diode loss respectively.

$$P_o = 19.29 \ \frac{mW}{Cm^2}$$

or changing units

$$P_o = 17.92 \ \frac{watts}{ft^2}$$

For an N KW concentrated system, the area A of cells required can be calculated from the following:

$$N \times 1000 = A \times P_o \times C_e \times \frac{Nt}{N_o}$$

where C_e = the effective concentration ratio, which is obtained from C_g x RE where RE is the reflection efficiency as obtained in Reference 1.

N_t = cell efficiency at the operating temperature

N_o = cell efficiency at the temperature for which P_o was computed (55°C)

$$A = \frac{(0.166)(1000)N}{(17.92)C_e N_t}$$

for 5 KW arrays, $N = 5$ and $A = \frac{46.317}{C_e N_t}$

for 20 KW arrays, $N = 20$ and $A = \frac{185.268}{C_e N_t}$

For each of these size arrays, the area required is a function of selected mirror tilt angle ϕ , since RE, temperature, and concentration ratio are functions of ϕ and N_t is a function of temperature.

The results are shown in Table 6.1-1 for mirrors using vapor deposited aluminum (VDA) for the reflective surface and in Table 6.1-2 for mirrors employing a "cold mirror" reflective surface.

6.2 Silicon Arrays

All calculations in this section are identical to those described in Section 6.1.

At $55^{\circ}C$ with winter solstice condition, $N_o = 11.2\%$

$$P_o = 135.3 \times 1.03 \times .112 \times .90 \times .97 \times .96 \times .995 \frac{mV}{Cm^2}$$

$$P_o = 12.09 \frac{watts}{ft^2}$$

$$A = \frac{46.319}{C_e N_t} \text{ for 5 KW systems}$$

$$A = \frac{185.299}{C_e N_t} \text{ for 20 KW systems}$$

The results are shown in Tables 6.2-1 for VDA coated mirrors and 6.2-2 for improved cold mirror coated mirrors.

TABLE 6.1-1

REQUIRED ARRAY SIZE VERSUS MIRROR TILT ANGLE, $\emptyset$, FOR VDA COATED MIRRORS, GaAs SOLAR CELLS

$\emptyset$ degrees	C_g	RE	T_{oC}	N_t %	Ratio, Mirror Height to Array Width l	5 KW System A ft^2	20 KW System A ft^2
50	1.35	0.94	32	17.5	.45	208.6	834.2
55	1.68	0.92	50	16.8	.84	178.4	713.5
60	2.00	0.90	64	16.2	1.36	158.8	635.3
65	2.28	0.88	78	15.7	2.07	147.0	588.1
67.5	2.41	0.88	86	15.4	2.55	141.8	567.2
68.0	2.51	0.87	88	15.3	3.07	138.6	554.5
70.0	2.88	0.86	97	15.0	4.16	124.7	498.7
75.0	3.73	0.82	123	13.9	8.52	108.9	435.8
76.0	4.09	0.81	130	13.6	11.10	102.8	411.2
77.0	4.45	0.79	136	13.4	13.70	98.3	393.3
78.75	5.03	0.77	150	12.8	20.04	93.4	373.7

TABLE 6.1-2

REQUIRED ARRAY SIZE VERSUS MIRROR TILT ANGLE, Ø, FOR MIRROR WITH "IMPROVED COLD MIRROR" COATING, GaAs SOLAR CELLS

Ø degrees	C_g	RE	T_{oC}	N_t %	Ratio, Mirror Height to Array width 1	5 KW System A ft^2	20 KW System A ft^2
50	1.35	0.92	28	17.6	.45	211.9	847.6
55	1.68	0.88	40	17.4	.84	180.0	720.0
60	2.00	0.85	51	16.7	1.36	163.1	652.4
65	2.28	0.83	60	16.4	2.07	149.2	596.8
67.5	2.41	0.825	67	16.2	2.55	143.8	575.2
68	2.51	0.82	69	16.1	3.07	139.8	559.2
70	2.88	0.79	75	15.8	4.16	128.8	515.2
75	3.73	0.74	94	15.0	8.52	111.9	447.6
76	4.09	0.72	99	14.9	11.10	105.5	422.0
77	4.45	0.71	104	14.6	13.70	100.4	401.6
78.75	5.03	0.67	115	14.2	20.04	96.8	387.2

TABLE 6.2-1 - REQUIRED ARRAY SIZE VS MIRROR TILT ANGLE Ø FOR VDA COATED MIRRORS, Si SOLAR CELLS

Ø degrees	Ratio, Mirror Height to Array width l	C_g	RE	T ^oC	N_t	5 KW System A ft^2	20 KW System A ft^2
50	.45	1.35	.94	48	11.6	314.6	1258.6
55	.84	1.68	.92	72	10.1	296.7	1186.9
60	1.36	2.00	.90	85	9.2	279.7	1118.8
65	2.07	2.28	.88	99	8.3	278.1	1112.6
67.5	2.55	2.41	.88	108	7.7	283.6	1134.6
68	3.07	2.51	.87	110	7.5	282.8	1135.8
70	4.16	2.88	.86	119	7.0	267.1	1068.6
75	8.52	3.73	.82	146	5.2	291.2	1164.9
76	11.10	4.09	.81	153	4.8	291.2	1165.1
77	13.7	4.45	.79	-	-	-	
78.75	20.04	5.03	.77	-	-	-	

TABLE 6.2-2 - REQUIRED ARRAY SIZE VS MIRROR TILT ANGLE Ø FOR IMPROVED COLD MIRROR COATED MIRRORS, Si SOLAR CELLS

Ø degrees	1	C_g	RE	T ^oC	N_t	5 KW System A ft^2	20 KW System A ft^2
50	.45	1.35	.92	44	11.8	316.0	1264
55	.84	1.68	.88	57	11.0	284.8	1139
60	1.36	2.00	.85	71	10.1	269.8	1079
65	2.07	2.28	.83	82	9.4	260.4	1041.6
67.5	2.55	2.41	.825	89	8.9	261.7	1046.8
68	3.07	2.51	.82	90	8.8	255.7	1022.8
70	4.16	2.88	.79	98	8.3	245.3	981.2
75	8.52	3.73	.74	118	7.0	239.7	958.8
76	11.10	4.09	.72	123	6.7	234.8	939.2
77	13.70	4.45	.71	129	6.3	232.7	930.8
78.75	20.04	5.03	.67	139	5.6	245.4	981.6

7.0 MECHANICAL DESIGN, STRESS, & MASS PROPERTIES

7.1 Design Criteria

The primary objective in this design is to optimize the power-to-mass ratio. Therefore, it is desirable to keep the structure as simple as possible.

The Hughes Flexible Rolled-up Solar Array (FRUSA) was chosen as the baseline solar panel. The FRUSA is a flight proven design in which a light weight blanket consisting of a kapton substrate covered with solar cells is rolled up on a drum. The blanket is deployed by a pair of motor driven beryllium-copper bi-stems. This design was chosen because it is a demonstrated design, highly weight efficient, packages very compactly and is simply deployed.

The geometry for the baseline design was taken from knowledge gained in the previous phases of this study. The basic configuration is a two wing v-trough concentrator system, with 1/3 mil kapton mirrors. An aspect ratio (length/width) of 3 was chosen for the solar panel. A geometric concentration ratio (C_G) of 2.5 appeared to be optimum. This yields a mirror tilt angle (θ) of 68° from the horizontal and a mirror height of approximately 3 times the panel width.

In designing the mirror support structure, the approach taken was that the mirrors and mirror support structure should stow across the FRUSA in the predeployed condition such that the stowage envelope dimensions would not be substantially increased due to the mirror assemblies. A few of the considered support/stowage schemes are listed below.

Structure Concepts	Reasons for Rejection or Acceptance
Telescoping T-shaped support structure as proposed in Ref. 2.	Rejected: Complicated, not weight efficient
Individual mirror panels with "Kite type" structure	Rejected: Complicated stowage necessary. Too heavy.
A three segment boom at each end of each mirror. Booms fold down along the FRUSA width.	Accepted: Simple, lightweight.

Mirror Folding Concepts	Reasons for Rejection or Acceptance
Mirrors festooned (accordian folded) onto solar panel and rolled up with panel onto drum as proposed in Ref. 2.	Rejected: Difficult to attach supports to mirrors. Damage to mirror likely.
Mirrors folding down in thirds along the panel length and then folding in thirds with the creases parallel to the panel width.	Reject: Difficult to stow safely and difficult to deploy.
Each mirror divided into three segments corresponding to the three boom segments and rolled up on the booms.	Accepted: Mirrors well protected and stowed. Simple light weight deployment.

7.2 Baseline Design

An overall sequential view of the baseline design is shown in Appendix A, Drawing No. 1, "Deployment Scenario". To best understand the function of the design, it is helpful to follow through the deployment in reverse, starting with the fully deployed panel, Dwg. No. 1 (view 6), and working back to the stowed configuration. Drawing 1. (View 6). The FRUSA is unrolled and held between the stowage drum and the spreader bar. Beryllium-copper bi-stems connect the two. At each corner of the solar panel are graphite/epoxy tubular booms which extend at the proper angle. Each boom is composed of three segments. The segments are connected by aluminum fittings, with springloaded hinges for deployment from the stowed position and latches to hold the unfolded booms in the deployed position. The hinge-lock scheme is shown in Drawing No. 2. The inboard booms attach at the base to the FRUSA assembly structure. The outboard booms are attached to the spreader bar. The mirrors on each side of the panel are actually three separate mirror segments. The mirror segments are stretched between corresponding boom segments.

(View 5). In this view, a motor is driving the bi-stems out of their housings, pushing the spreader bar out. The spreader bar draws out the solar array, the outboard booms, and, therefore, the mirrors with it. The solar array is unrolling from its stowage drum, and the mirrors are unrolling from the inboard boom segments. The mirrors are actually rolled on teflon sliptubes which are around the inboard boom segments but are allowed to rotate with respect to the fixed booms, as the mirrors are unrolled.

(View 4). The solar array is completely stowed on the drum and the mirrors are rolled onto the inboard boom segments. Note that the booms on the left side of the FRUSA, in this view, are next to each other while the booms on the right are far enough apart to permit the left side booms to fit between them.

(Views 3 and 2). These views show the booms deploying from their folded positions. This deployment is driven by springs at each of the hinge points. The right side booms deploy first because in the stowed position they fit on both sides of the left side booms, with their mirrors passing over the left side booms. The right side booms are allowed to deploy by firing a cable cutter. When the first set of booms lock in position, a latch is automatically released which allows the second set to deploy.

(View 1). All parts are stowed and locked in position for launch.

This now brings us to the launch lock detail, Drawing No. 3. The view on the left in this drawing is an end view of the FRUSA with the bi-stem housing removed and the mirror support booms stowed and locked in place. The outside booms, which have their hinged base on the far side in this view are held against the attach fittings by a cable. The inside booms, which are based on the near side as shown, are constrained on the far side by a loop which is released automatically when the outside booms are deployed. The passive restraint loop shown is necessary to prevent the top two segments from unfolding as a unit. When the top segment of the booms rotate up on deployment, they unhook from the loop allowing the boom deployment to continue. With all the booms deployed and latched, the bi-stems extend, thus unrolling the blanket and the mirrors, completing the scenario previously described.

Finally, the last Drawing, No. 4, depicts one method of providing uniform tension in the mirror. This tension, approximately 1.67×10^2 lbs/in, is necessary to retain a flat reflective surface. The drawing is self-explanatory.

7.3 Sizing Criteria and Methods

Since the FRUSA is a flight proven device, stress analysis for sizing was not required. Instead, the sizes and weights were extrapolated from the existing FRUSA design using criteria outlined in the next section.

The largest, and by far heaviest, components of the mirror assembly are the graphite-epoxy support booms. These booms must be examined in both stowed and deployed conditions.

Envisioning an STS launch, a conservative launch load of 10gs in any direction was imposed. A fundamental resonant frequency, for the stowed boom segments, of 15Hz or more was also taken as a design objective, a criterion used in the original FRUSA design. Both of these constraints are intentionally conservative.

Note that in sizing the booms by stiffness, if the weight of the mirrors on the booms is ignored, the frequency is independent of the wall thickness. Even when the mirrors are included in the calculations, the thickness is a secondary effect. Therefore, it is desirable to use the minimum possible thickness. Considering an omni directional graphite fiber lay-up, allowing for epoxy thickness, and being conservative again, a thickness of .05 in. was assumed and is believed to be a reasonable figure.

It appears that this stiffness criteria is the most demanding; therefore, the calculations to follow will assume the boom radius-to-panel width relationship shown in Figure 7.3.1.

BOOM SIZING by STIFFNESS

Mass of BOOM $= \frac{\pi (R^2 - r^2) \ell (\rho_G)}{g}$

$M_b \approx \frac{2\pi R t \ell \rho_G}{g}$

Aspect Ratio of 3/1

Mass of MIRRORS $= \frac{\ell^2 (.0003) \rho_K}{g}$

$\rho_G = \rho_K = .06 \ lbs/in^3$

$I = \pi/4 (R^4 - r^4)$

$= 1/4 A (R^2 - r^2)$

$\approx 1/4 \, 2\pi R t (2R^2)$, SMALL WALL APPROXIMATION

$\approx \pi R^3 t$

ℓ = PANEL WIDTH
t = WALL THICKNESS
R = BOOM RADIUS

$f_n = \frac{9.87}{2\pi} \sqrt{\frac{EI}{m \ell^3}}$

ASSUME A SIMPLY SUPPORTED BEAM

FIRST ORDER APPROXIMATION: IGNORE MIRRORS

$\sqrt{\frac{EI}{m_\ell 3}} = \sqrt{\frac{E \pi R^3 t}{2\pi R t \ell^4 \rho_G} g} = \sqrt{\frac{E R^2 g}{2 \ell^4 \rho_G}}$

$E = 42 \times 10^6$ PSI

$R = 6 \times 10^{-6} \ell^2 f_n$ at $f_n = 15Hz$ $R = 9 \times 10^{-5} \ell^2$

"INCLUDE MIRROR

$f_n = \frac{9.87}{2\pi} \sqrt{\frac{EI}{(m_b + m_k) \ell^3}}$

$R^3 = 3.58 \times 10^{-11} f_n^2 \ell^4 R + 1.908 \times 10^{-15} \ell^5 f_n^2 / t$

INSERT $f_n = 15Hz$ $t = .05in$

$R = 1.036 \times 10^{-4} \ell^2 \cos\left(\frac{\cos^{-1}\left(\frac{30.81}{\ell}\right)}{3}\right)$

FOR THE WIDTHS OF INTEREST THIS EQUATION IS GRAPHED IN FIGURE 7.3.1

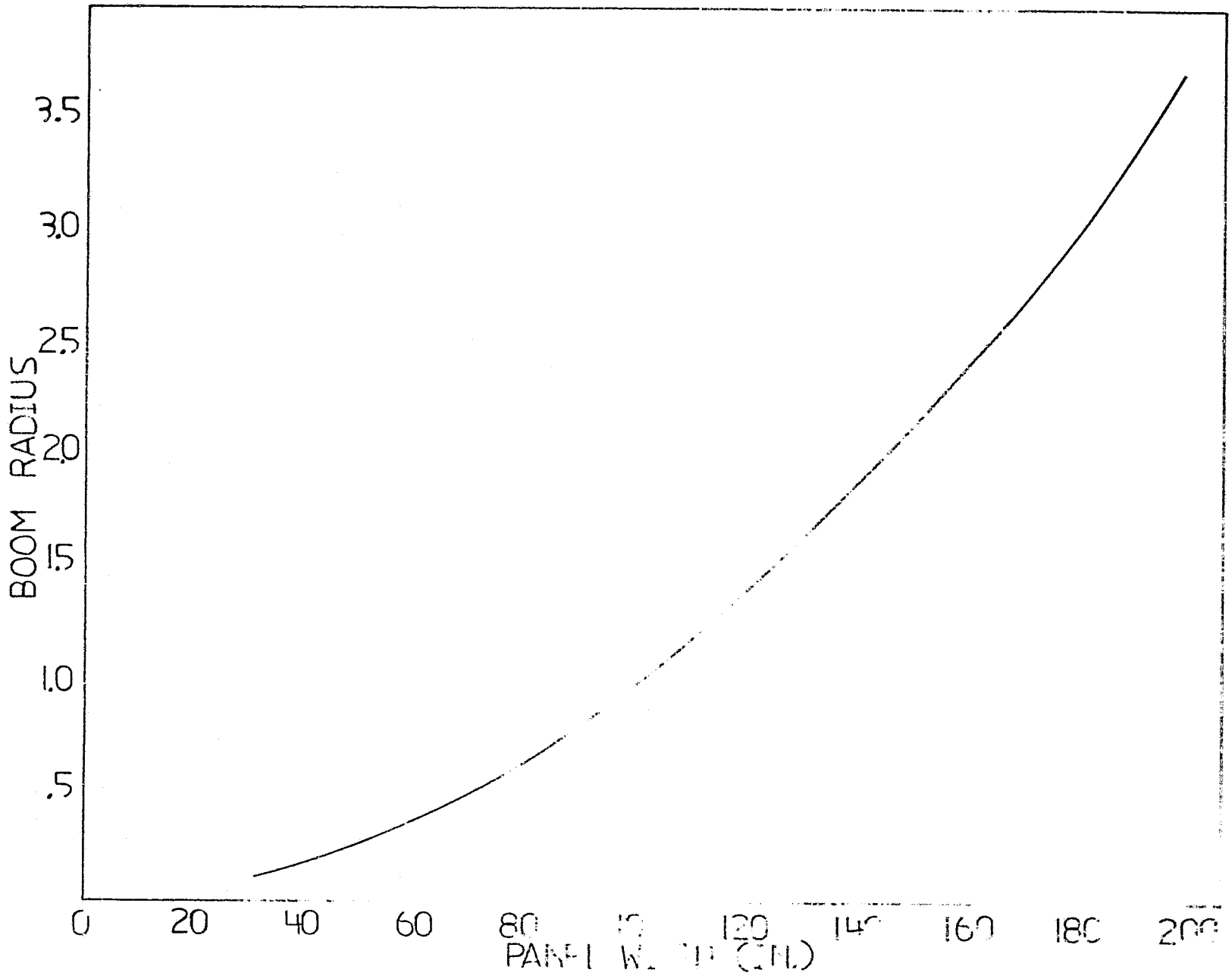

FIGURE 7.3.1

Boom Strength (Stowed)

$$M_{max} = \frac{w l^2}{8} \times 10g$$

$$\approx \frac{\pi R t l^2 \rho}{4} \times 10g$$

SMALL WALL APPROX.

$$I \approx \pi R^3 t$$

l = PANEL WIDTH

t = WALL THICKNESS

R = BOOM RADIUS

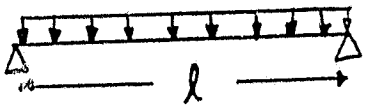

$$\sigma_{max} = \frac{MR}{I}$$

$$= \frac{\pi R^2 t l^2 \rho}{4\pi R^3 t} \times 10g$$

$$= \frac{l^2}{4R} \rho \times 10g$$

$$\rho = .06 lbs/in^3$$

$$R \sim l^2 \times 10^{-4}$$

$$\sigma_{max} = \frac{\rho \times 10g}{4 \times 10^{-4}} = 1500 psi$$

Tensile Strength of GY70 GRAPHITE $= 9 \times 10^4$ PSI

Boom Strength, Deployed

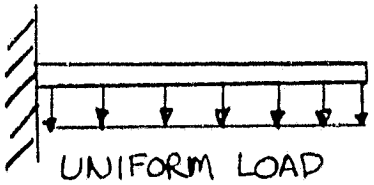

$T_{S_{KAPTON}} = 25\ KPSI$

$t_{KAPTON} = .000\bar{3}\ in.$

Max. LINEAR LOAD $= 3.\bar{3}\ lbs/in.$

$M_{max.} = \frac{w l^2}{2} = \frac{W l}{2}$

$I = \pi R^3 t$ small wall approx

$\sigma_{max} = \frac{MR}{I} = \frac{M R}{\pi R^{\cancel{3}2} t}$

$= \frac{w l^2}{2\pi R^2 t}$

$R^2 \sim 1.23 \times 10^{-10} l^4$ FROM STIFFNESS EQUATIONS

$\sigma_{max} = \frac{w}{2\pi (1.23 \times 5^{-10}) l^4 t}$

$\sigma_{max} = \frac{2.16 \times 10^{11}}{l^4}$

$T_{S_{Graphite}} = 90\ KPSI$

∴ The Boom is Stronger than the Kapton as long as the Boom Length is $> \underline{40 in}$ which is always True.

Boom Natural Frequency, Deployed

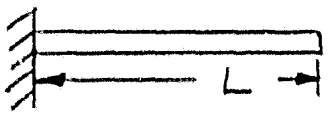

$$f_n = \frac{3.52}{2\pi}\sqrt{\frac{EIg}{wL^4}}$$

$I = \pi R^3 t$ } small wall approx.
$w = 2\pi R t \rho$ }

$$= \frac{3.52}{2\pi}\sqrt{\frac{E\pi R^3 t g}{2\pi R t L^4 \rho}}$$

$R^2 \approx \left(\frac{L}{3}\right)^4 \times 10^{-8}$ [From Boom Sizing]

$$f_n = \frac{3.52}{2\pi}\sqrt{\frac{E\pi L^4 g\,(1.23\times10^{-10})}{2\pi L^4 \rho}}$$

$$f_n = \frac{3.52}{2\pi}\sqrt{\frac{E g\,(1.23\times10^{-10})}{2\rho}}$$

$E = 42 \times 10^6$ lbs/in.^{2}
$\rho = .06$ lbs/in.^{2}
$g = 32.2$ ft/sec^2

$$\underline{f_n = .66\ \text{Hz}^*}$$

* Note: Frusa Stiffness Deployed $f_n = .25$ Hz

These calculations verify that indeed the stiffness of 15Hz for launch is the designing consideration. Therefore, Figure 7.3.1 will be used to size the booms.

7.4 Weight Analysis

7.4.1 FRUSA Sizing

Most of the FRUSA was scaled geometrically from existing flight design. The important exceptions were the bi-stems and their deployment mechanisms. The bi-stems were designed by stiffness as follows:

$$F_N \propto \frac{EI}{L^3 M} \qquad I \propto R^4$$

E, F_N AND R/t ARE CONSTANT

$$\therefore R \propto \sqrt[4]{L^3 M}$$

$$\therefore W \propto \sqrt{L^5 M}$$

The deployment mechanism weight was determined from a graph of deployer weight versus bi-stem diameter. The weights were estimated by extrapolating the weights on both the FRUSA parts and mirror assemblies, including the hardware and small parts. The extrapolation approach yields results which are believed to be reasonably accurate.

7.4.2 Weights

The weight summaries for 5Kw and 20Kw systems, silicon and gallium arsenide solar cells, with both vapor deposited aluminum and cold mirror surfaces appear in Tables 7.4.1 - 7.4.6. Several geometric concentration ratios are considered in each table. There is no differentiation made between VDA and cold mirror versions for the gallium arsenide system because the required solar panel areas were found in Section 6 to be virtually identical.

There was some concern that in the large area versions, the assumed length to width aspect ratio of 3 for the solar panels might not be optimum. Figure 7.4.1 is graph of weight vs. aspect ratio for the largest version: the 20 KW, silicon, VDA, baseline design. This figure demonstrates that the ratio used on the baseline design (3) is in fact close to optimum. On the smaller area versions, the effect would be even more pronounced.

7.5 Power to Mass Results

The power to mass results are summarized in Figure 7.5.1 and 7.5.2.

The two gallium arsenide systems perform quite well, providing a 42 percent increase in power-to-mass ratio (114 watts/Kg) at the optimum concentration ratio. This optimum occurs at a C_G of approximately 2.9 instead of the assumed ratio of 2.5. It is difficult to pinpoint the optimum exactly. The data points would not fit a smooth curve because the baseline design requires boom segments that have lengths that are near integral multiples of the panel width. So a small increase in C_G may require another boom segment to be added, thus greatly increasing the weight.

At $C_g = 1$, the values shown are for an unconcentrated array without mirror assemblies. The initial dip in each curve is caused by the sudden inclusion of this mass before significant power increases are obtained.

The silicon systems did not fare nearly as well as the gallium arsenide systems. This is inevitable considering the minor area advantage gained by concentrating on the silicon panels. For 5Kw systems, small concentration ratios don't cause a power to mass penalty, therefore they may be advantageous from the standpoint of

solar cell cost savings. With the 20 KW systems, a power to mass penalty is required for any reduction in solar cell area or solar cell cost.

In general, smaller systems perform better from a power to mass standpoint than do larger systems because the larger systems require a cubic increase in boom weight with respect to the increased panel width.

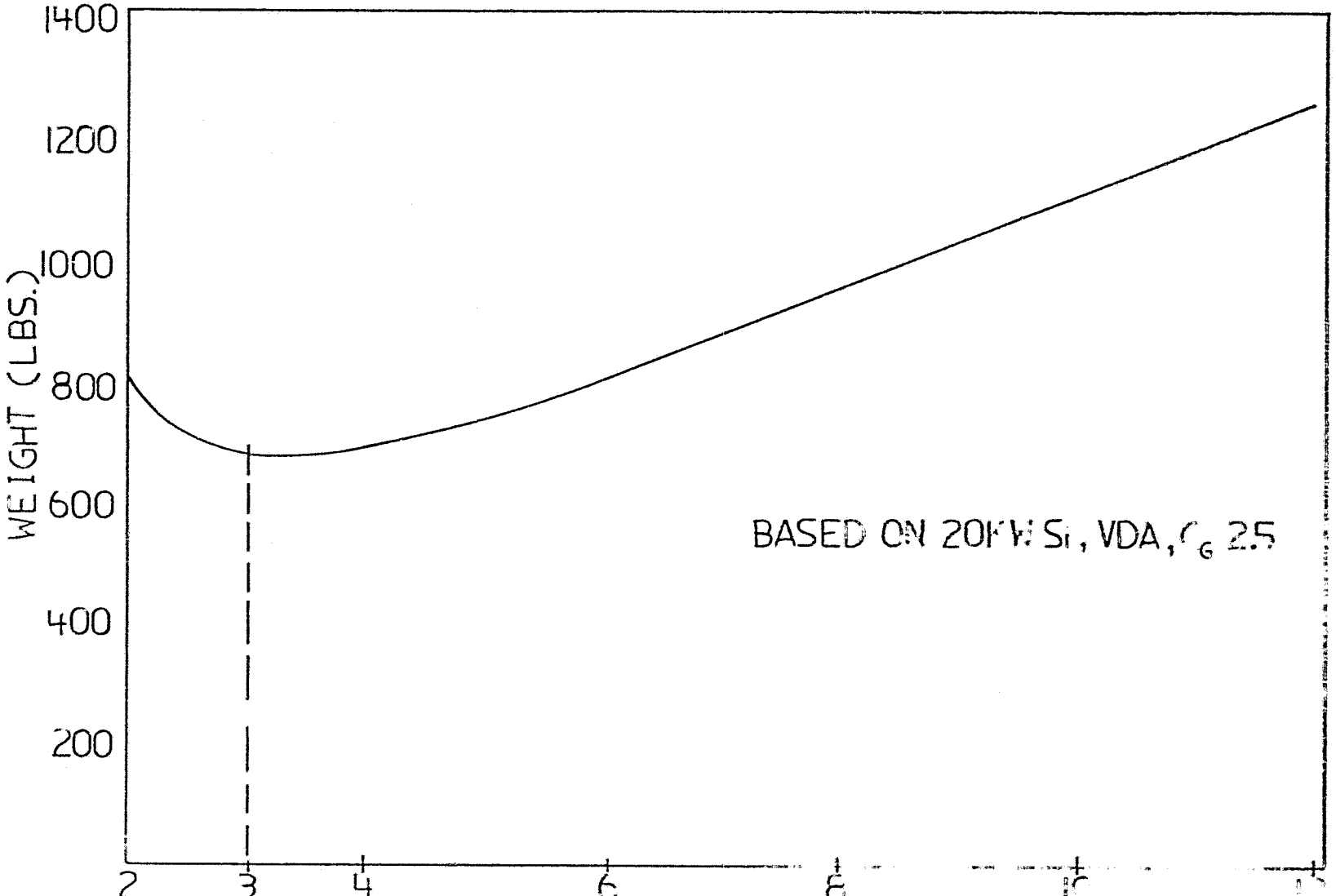
1400
1200
1000
800
600
400
200
WEIGHT (LBS.)
BASED ON 20K W, S, VDA, C 2.5
2
3
4
6
8
ASPECT RATIO (L/W)

FIGURE 7.4.1

C_G	FRUSA ASSY.				MIRROR ASSY.			TOTALS	
	Solar Panel W(lbs) (Area (ft^2))	Bi-Stem and Deployer W(lbs) (d(in))	Drum Assembly W(lbs)	Misc. W(lbs)	Boom Assembly W(lbs) (d(in))	Mirror W(lbs)	Fittings and Hardware W(lbs)	Weight (lbs) (Kg)	Power/Weight Watts/lbs Watts/Kg
2.00	42.3 (279.7)	15.4 (1.1)	33.5	7.9	16.3 (1.3)	2.2	3.8	121.4 55.2	41.2 90.6
2.51	42.8 (282.8)	17.1 (1.2)	33.7	7.9	24.5 (1.3)	4.9	6.1	137.0 62.3	36.5 80.3
2.88	40.4 (267.1)	16.9 (1.2)	32.7	7.6	25.6 (1.2)	6.2	7.5	136.9 62.2	36.5 80.4
4.09	44.0 (291.2)	23.9 (1.4)	34.2	8.1	89.8 (1.4)	18.5	20.3	238.8 108.6	20.9 46.1
Unconc. with no mirrors	53.9 (356.3)	18.6 (1.2)	37.8	9.6		0		119.9 54.5	41.7 91.7
Unconc. with mirrors C_G=1	53.9 (356.3)	19.8 (1.3)	37.8	9.6	11.3 (1.62)	2.1	4.0	138.5 63.0	36.1 79.4

TABLE 7.4.1

Si 5Kw VSA

C_G	FRUSA ASSY.				MIRROR ASSY.			TOTALS	
	Solar Panel W(lbs) (Area (ft^2))	Bi-Stem and Deployer W(lbs) (d(in))	Drum Assembly W(lbs)	Misc. W(lbs)	Boom Assembly W(lbs) (d(in))	Mirror W(lbs)	Fittings and Hardware W(lbs)	Weight (lbs) (Kg)	Power/Weight Watts/lbs Watts/Kg
2.00	40.8 (269.8)	14.8 (1.1)	32.9	7.6	14.4 (1.25)	2.1	3.7	116.3 52.9	43.0 94.6
2.51	38.6 (255.7)	14.6 (1.1)	32.0	7.3	19.2 (1.2)	4.4	5.8	121.9 55.4	41.0 90.2
2.88	37.1 (245.3)	14.5 (1.1)	31.4	7.1	25.0 (1.14)	5.8	7.0	127.9 58.1	39.1 86.0
4.09	35.5 (234.8)	16.9 (1.2)	30.7	6.8	66.0 (1.12)	15.0	17.6	188.5 85.7	26.5 58.4
Unconc. with no mirrors	53.9 (356.3)	18.6 (1.2)	37.8	9.6		0		119.9 54.5	41.7 91.7
Unconc. with mirrors C_G=1	53.9 (356.3)	19.8 (1.3)	37.8	9.6	11.3 (1.62)	2.1	4.0	138.5 63.0	36.1 79.4

TABLE 7.4.2

Si 5KW COLD MIRROR

C_G	FRUSA ASSY.				MIRROR ASSY.			TOTALS	
	Solar Panel W(lbs) (Area (ft^2))	Bi-Stem and Deployer W(lbs) (d(in))	Drum Assembly W(lbs)	Misc. W(lbs)	Boom Assembly W(lbs) (d(in))	Mirror W(lbs)	Fittings and Hardware W(lbs)	Weight (lbs) (Kg)	Power/Weight Watts/lbs Watts/Kg
2.00	169.2 (1118.8)	137.8 (2.9)	67.1	25.2	128.1 (5.0)	8.8	23.4	560.0 254.4	35.7 78.6
2.51	171.7 (1135.8)	152.7 (3.0)	67.5	25.5	199.4 (5.0)	19.6	34.9	671.3 305.1	29.8 65.5
2.88	161.6 (1068.6)	148.7 (3.0)	66.0	24.5	236.6 (4.8)	26.0	46.6	701.0 322.7	28.2 62.0
4.09	176.2 (1165.1)	237.3 (3.8)	68.4	26.1	726.0 (5.1)	73.8	127.3	1435.1 652.3	13.9 30.7
Unconc. with no mirrors	215.5 (1425.2)	150.8 (2.9)	75.6	31.2		0		473.1 215.0	42.3 93.0
Unconc. with mirrors C_G=1	215.5 (1425.2)	187.4 (3.7)	75.6	31.2	87.9 (6.3)	8.2	34.2	640.0 290.1	31.3 68.9

TABLE 7.4.3

Si 20Kw VDA

C_G	FRUSA ASSY.				MIRROR ASSY.			TOTALS	
	Solar Panel W(lbs) (Area (ft^2))	Bi-Stem and Deployer W(lbs) (d(in))	Drum Assembly W(lbs)	Misc. W(lbs)	Boom Assembly W(lbs) (d(in))	Mirror W(lbs)	Fittings and Hardware W(lbs)	Weight (lbs) (Kg)	Power/Weight Watts/lbs Watts/Kg
2.00	163.2 (1079.2)	121.8 (2.8)	65.8	24.4	118.3 (4.8)	8.5	23.3	525.3 238.8	38.1 83.8
2.51	154.6 (1022.8)	119.7 (2.8)	64.1	23.3	164.1 (4.6)	17.7	30.9	574.4 261.1	34.8 76.6
2.88	148.4 (981.2)	131.5 (2.9)	62.8	22.5	204.3 (4.5)	22.6	35.9	627.1 285.1	31.9 70.2
4.09	142.0 (939.2)	163.0 (3.3)	61.4	21.6	521.5 (4.2)	59.5	94.8	1063.8 483.6	18.8 41.4
Unconc. with no mirrors	215.5 (1425.1)	150.8 (2.9)	75.6	31.2		0		473.1 215.0	42.3 93.0
Unconc. with mirrors C_G=1	215.5 (1425.2)	187.4 (3.7)	75.6	31.2	87.9 (6.3)	8.2	34.2	640.0 290.1	31.3 68.9

TABLE 7.4.4

Si 20Kw COLD MIRROR

C_G	FRUSA ASSY.				MIRROR ASSY.			TOTALS	
	Solar Panel W(lbs) (Area (ft^2))	Bi-Stem and Deployer W(lbs) (d(in))	Drum Assembly W(lbs)	Misc. W(lbs)	Boom Assembly W(lbs) (d(in))	Mirror W(lbs)	Fittings and Hardware W(lbs)	Weight (lbs) (Kg)	Power/Weight Watts/lbs Watts/Kg
2.00	53.1 (158.8)	10.2 (.86)	25.2	5.0	7.3 (.75)	1.24 (431.9)	3.0	105.0 47.8	47.6 104.7
2.51	46.4 (138.6)	9.6 (.86)	23.6	4.5	9.1 (.66)	2.5 (851.0)	4.3	100.0 45.5	50.0 110.0
2.88	41.7 (124.7)	9.2 (.86)	22.4	4.2	10.5 (.60)	3.0 (1037.5)	5.2	96.2 43.7	52.0 114.4
4.09	34.4 (102.8)	8.7 (.78)	20.3	3.6	20.6 (.50)	6.6 (2282.1)	11.6	105.8 48.1	47.3 104.0
Unconc. with no mirrors	83.8 (250.4)	16.4 (1.2)	31.7	7.2		0		139.1 63.2	35.9 79.1
Unconc. with mirrors C_G=1	83.8 (250.4)	16.4 (1.2)	31.7	7.2	6.7 (1.15)	1.4	4.5	151.7 69.0	33.0 72.5

TABLE 7.4.5

GaAs 5Kw

C_G	FRUSA ASSY.				MIRROR ASSY.			TOTALS	
	Solar Panel W(lbs) (Area (ft^2))	Bi-Stem and Deployer W(lbs) (d(in))	Drum Assembly W(lbs)	Misc. W(lbs)	Boom Assembly W(lbs) (d(in))	Mirror W(lbs) (Area(ft^2))	Fittings and Hardware W(lbs)	Weight (lbs) (Kg)	Power/Weight Watts/lbs Watts/Kg
2.00	212.6 (635.3)	70.4 (2.30)	50.6	15.5	54.0 (2.9)	5.0 (1728.0)	10.3	418.4 190.2	47.8 105.2
2.51	185.5 (554.5)	59.7 (2.15)	47.3	13.8	69.3 (2.5)	9.8 (3404.6)	15.0	401.4 182.4	49.8 109.6
2.88	166.9 (498.7)	51.4 (2.05)	44.7	12.6	8.50 (2.3)	11.9 (4149.2)	18.1	390.6 177.5	51.6 112.7
4.09	137.6 (411.2)	45.7 (2.00)	40.7	10.75	160.4 (1.9)	26.3 (9128.6)	39.4	460.9 209.5	43.4 95.5
Unconc. with no mirrors	335.1 (1001.4)	121.3 (2.8)	63.4	22.9		0		542.7 246.7	36.9 81.1
Unconc. with mirrors C_G=1	335.1 (1001.4)	133.3 (2.9)	63.4	22.9	52.6 (4.5)	5.8	20.0	633.1 287.8	31.6 69.5

TABLE 7.4.6

GaAs 20Kw

FIGURE 7.4.1

ORIGINAL PAGE IS
OF POOR QUALITY

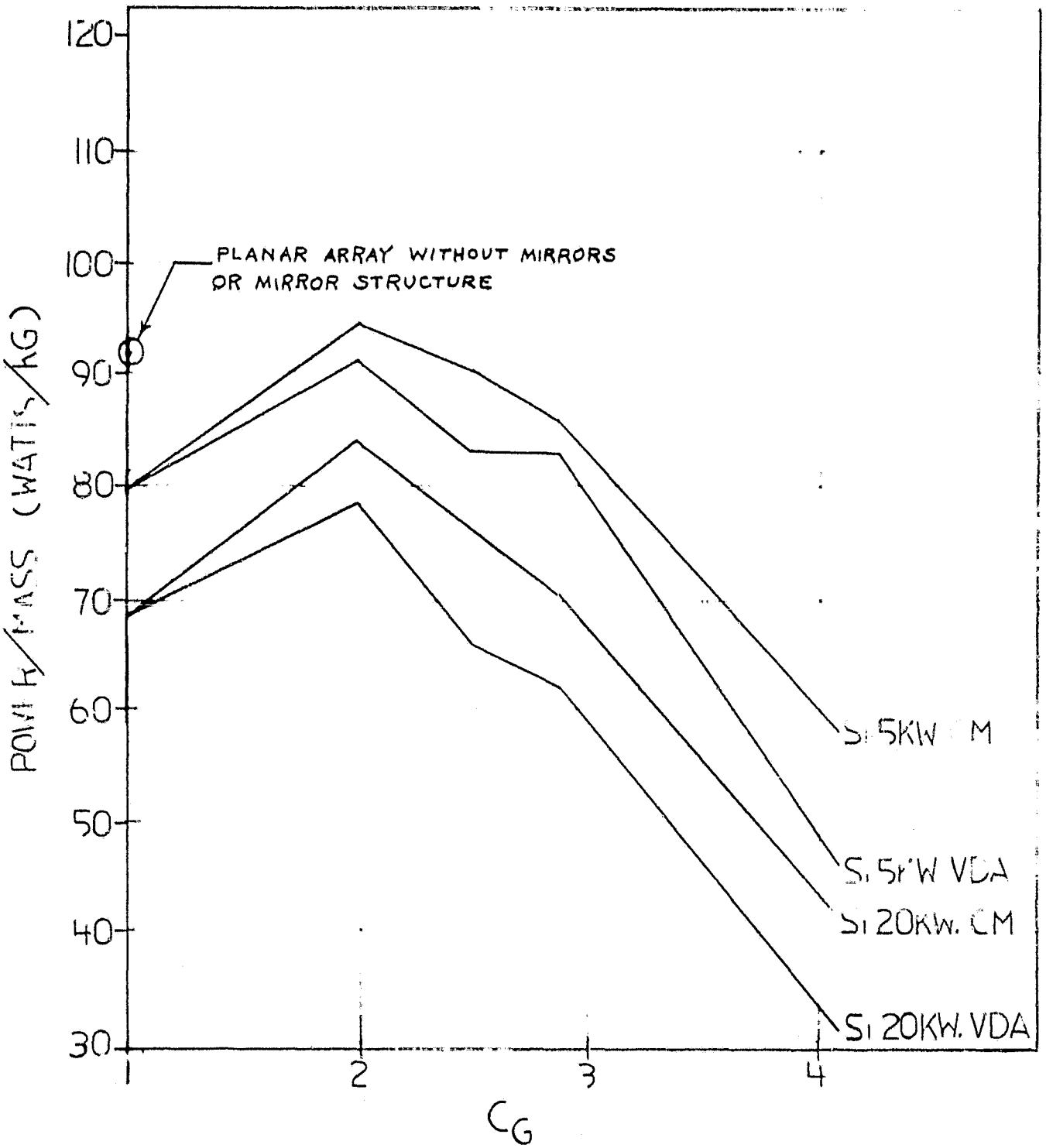

FIGURE 7.5.1

POWER TO MASS PERFORMANCE OF V-TROUGH CONCENTRATED Si ARRAYS

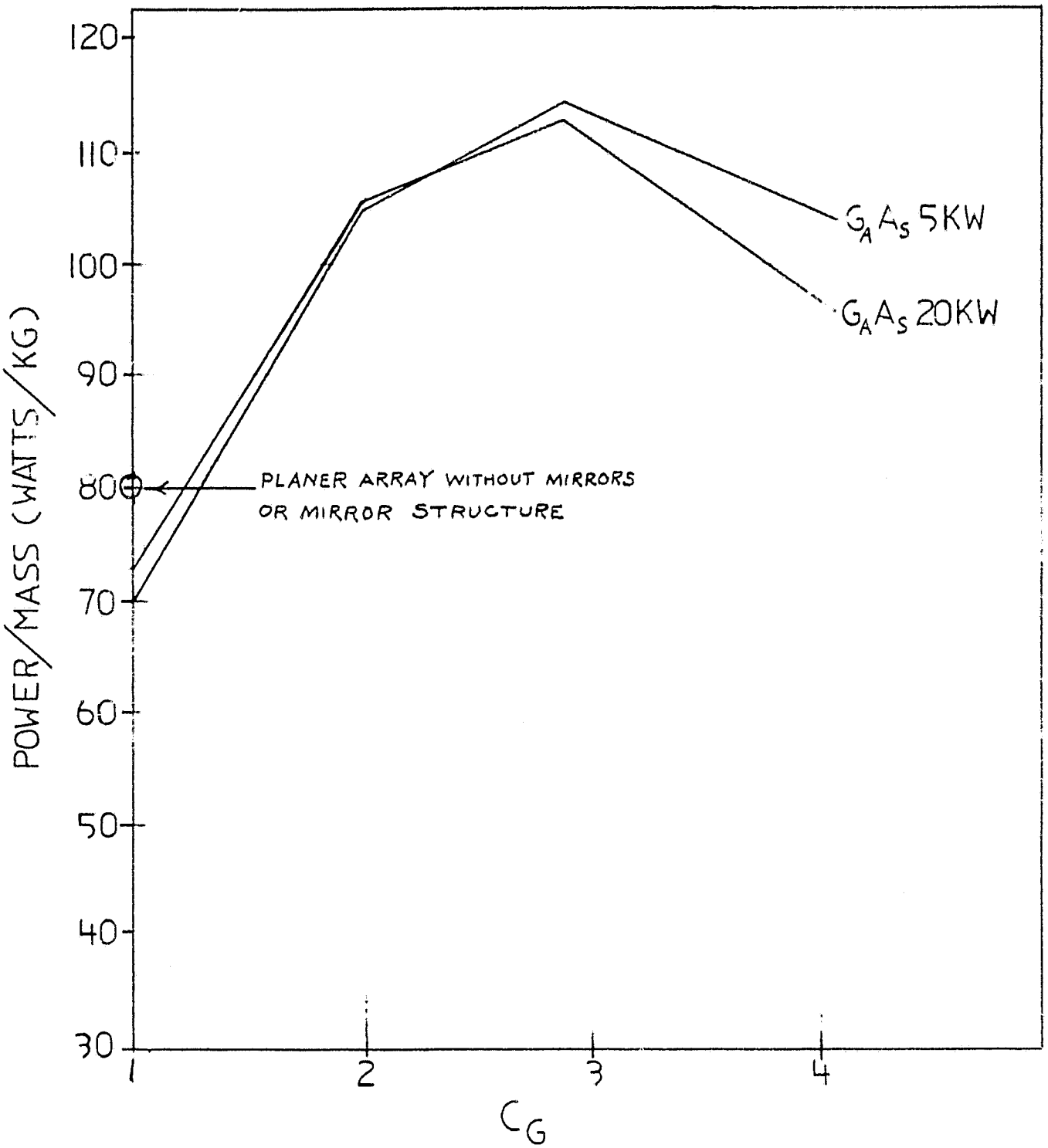

FIGURE 7.5.2

POWER TO MASS PERFORMANCE OF V-TROUGH CONCENTRATED GaAs ARRAYS

8.0 References

1. HAC Report, "Conceptual Design Study of Concentrator Enhanced Solar Arrays for Space Applications, Interim Final Report", Volume 1, Study Overview and Summary; Volume 2, Technical, 15 May 1979.

2. HAC Report "Conceptual Design Study of Concentrator Enhanced Solar Arrays for Space Application, Final Report of First Contract Extension Phase", 20 March 1980.

APPENDIX A

(Drawings No. 1, 2, 3 and 4)

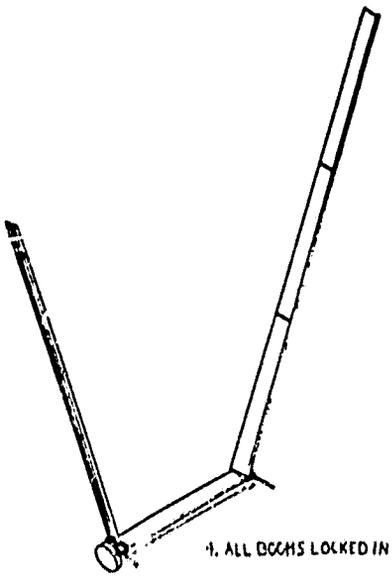

4. ALL BOOMS LOCKED IN PLACE.

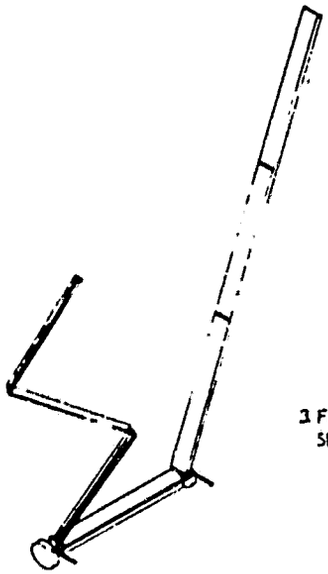

3 FIRST SET OF BOOMS LOCKED.
SECOND SET OF BOOMS DEPLOY

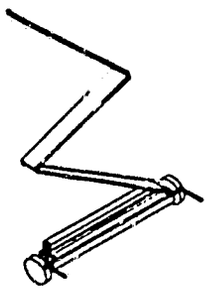

2. CABLE CUTTER FIRES
ALLOWING FIRST SET OF BOOMS TO DEPLOY

FOLDOUT FRAME

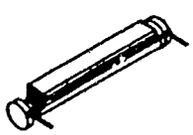

1. STOWED CONFIGURATION;
FRUSA ROLLED ON DRUM,
MIRRORS ROLLED ON BOOM SEGMENTS

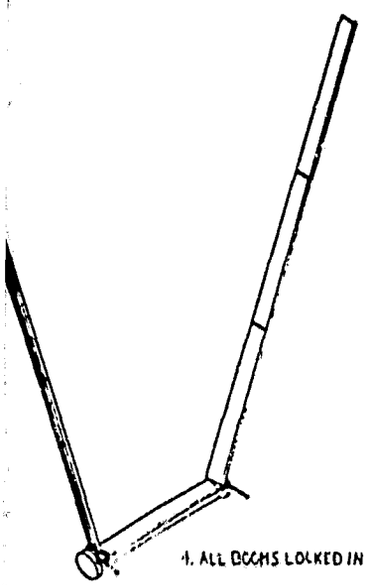

4. ALL BOOMS LOCKED IN PLACE.

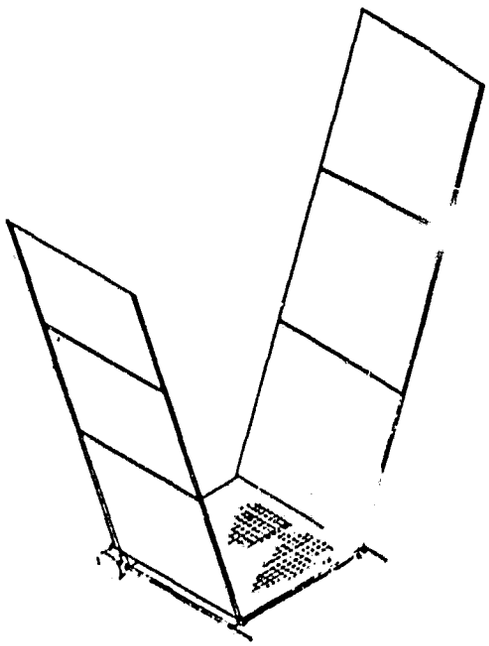

5. TRUSA UNROLLS DRAWING OUTBOARD BOOMS WITH IT. MIRRORS ROLL OFF INBOARD BOOMS ON TEFLON SLIPTUBES.

FOLDOUT FRAME 2

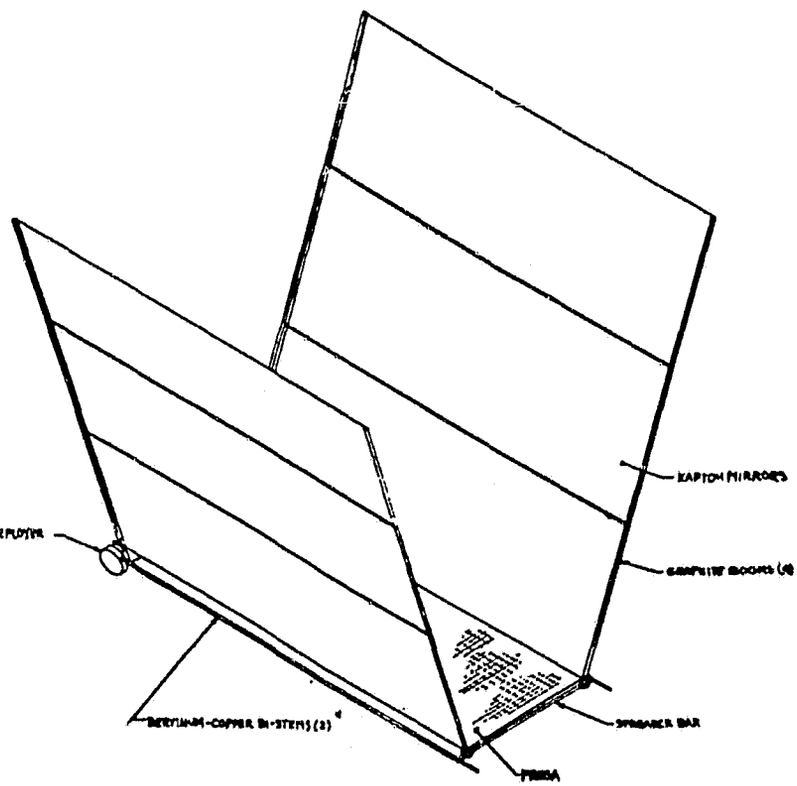

6. FULLY DEPLOYED.

QTY	FIGURE NO	PART NO OR IDENTIFYING NO	NOMENCLATURE OR DESCRIPTION	SPARE	ITEM OR FIGURE NO
			PARTS LIST		

UNLESS OTHERWISE SPECIFIED DIMENSIONS ARE IN INCHES AND PER ANSI Y14.5

.XXX	.XX	ANGLES
±.010	±.03	±0°30'

MATERIAL

CONTRACT

DR D.T.MORSE 3/1/80

CHK

APPD

HUGHES — HUGHES AIRCRAFT COMPANY CULVER CITY, CALIFORNIA

DEPLOYMENT SCENARIO, SOLAR CONCENTRATOR STUDY

SIZE E | FIGURE NO 82577 | DWG NO —

SCALE 1/2 | SHEET 1/1

NEXT ASSY | USED ON APPLICATION

FOLDOUT FRAME

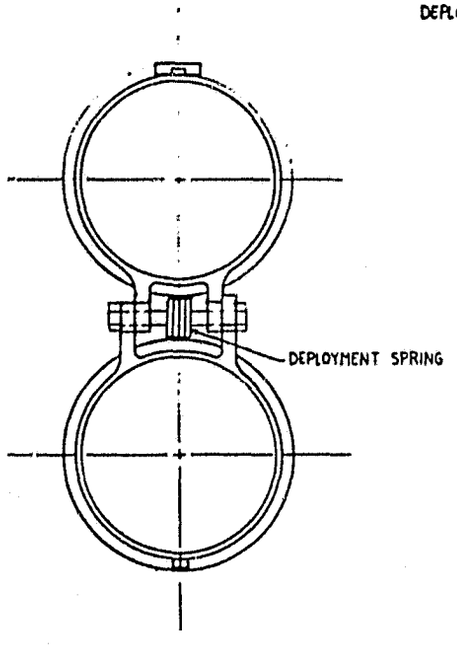

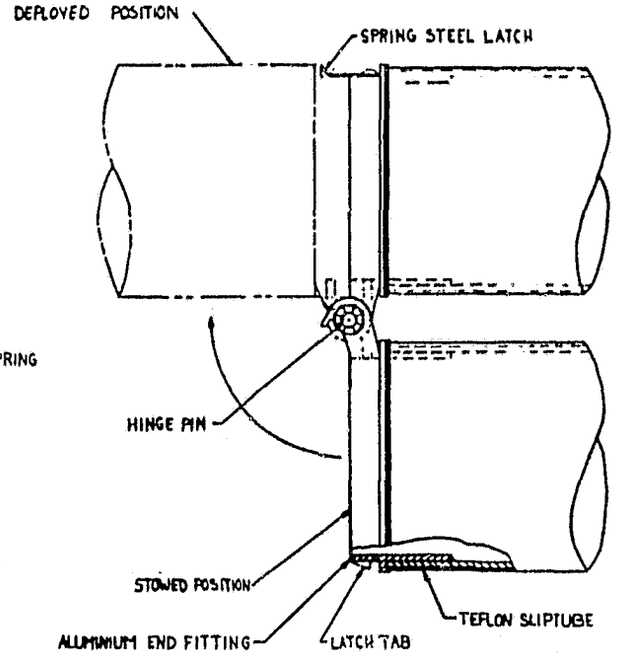

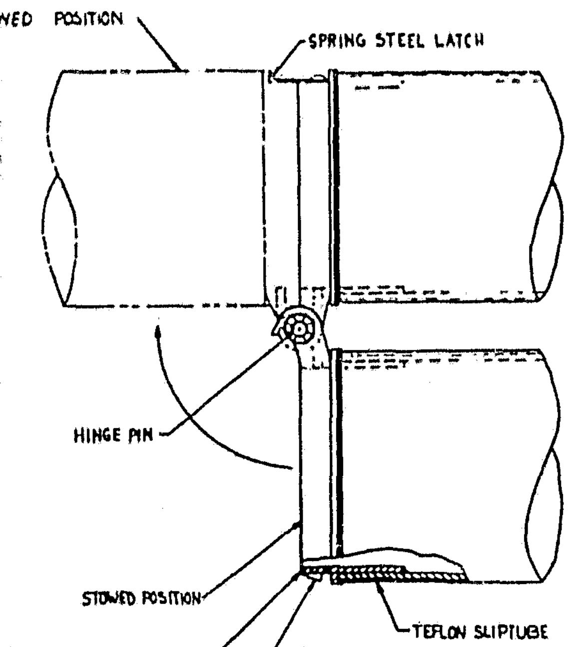

FOLDOUT FRAME 2

PARTS LIST

HUGHES AIRCRAFT COMPANY
CULVER CITY CALIFORNIA

UNLESS OTHERWISE SPECIFIED DIMENSIONS ARE IN INCHES AND PER ANSI Y14.5

HINGE / LOCK DESIGN
SOLAR CONCENTRATOR

SIZE	FSCM NO	DWG NO
E	82577	2

SCALE 2/1

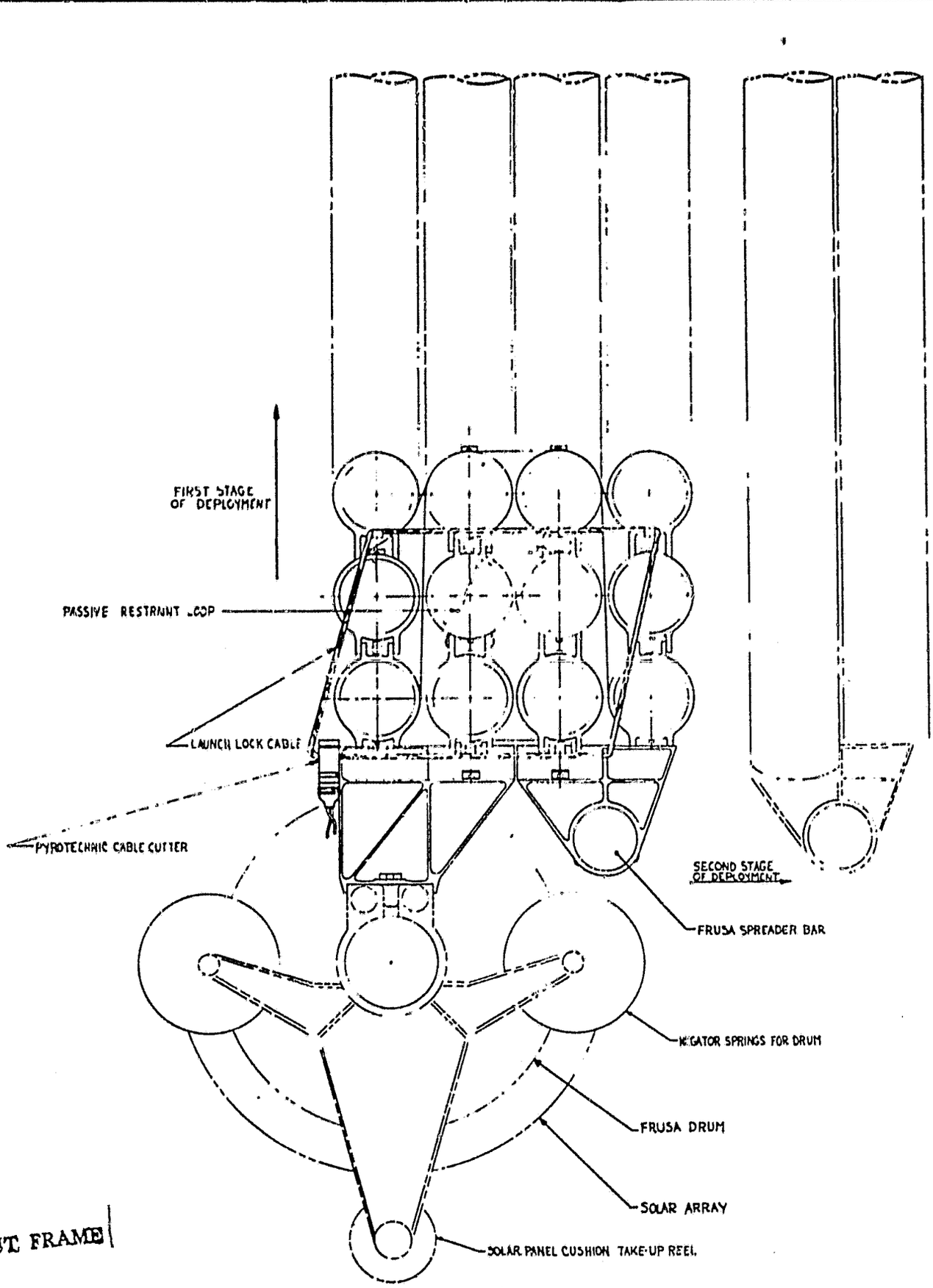

SECTION A-A

FOLDOUT FRAME

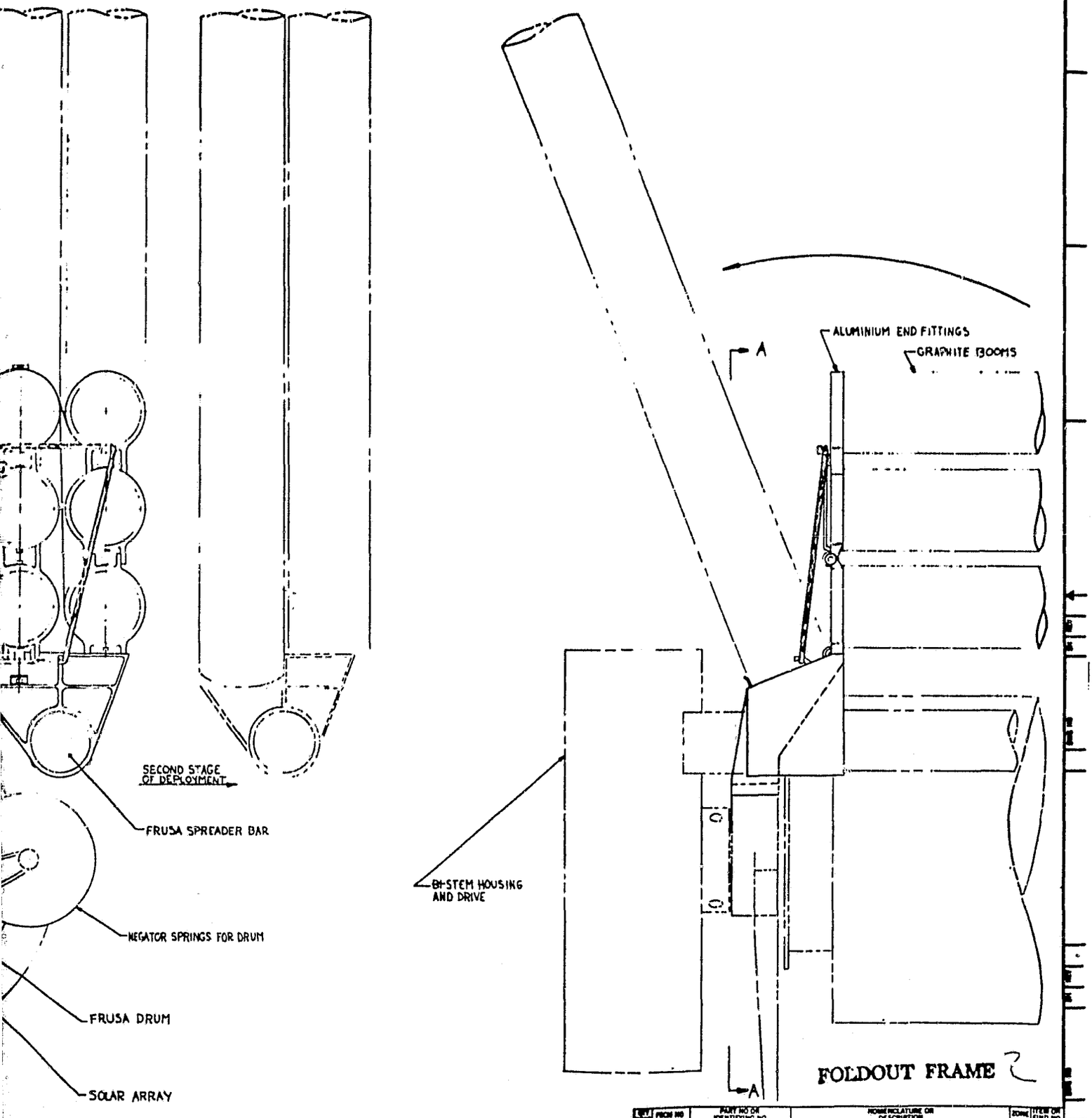

REVISIONS					
REV	AUTHORITY	ZONE	LTR	DESCRIPTION	DATE

QUANTITY	FSCM NO	PART NO OR IDENTIFYING NO	NOMENCLATURE OR DESCRIPTION	ZONE	ITEM OR FIND NO

PARTS LIST

UNLESS OTHERWISE SPECIFIED DIMENSIONS ARE IN INCHES AND PER ANSI Y14.5

.XX ± .030	.XX ± .05	ANGLES ± 0°30'

MATERIAL

CONTRACT

DRAWN G.J. MORSE DATE 6-20-80

CHK

APVD

HUGHES

HUGHES AIRCRAFT COMPANY
CULVER CITY, CALIFORNIA

LAUNCH LOCK SYSTEM,
SOLAR CONCENTRATOR STUDY.

SIZE	FSCM NO	DWG NO
E	82577	3

SCALE 1/1 SHEET

NEXT ASSY	USED ON
APPLICATION	

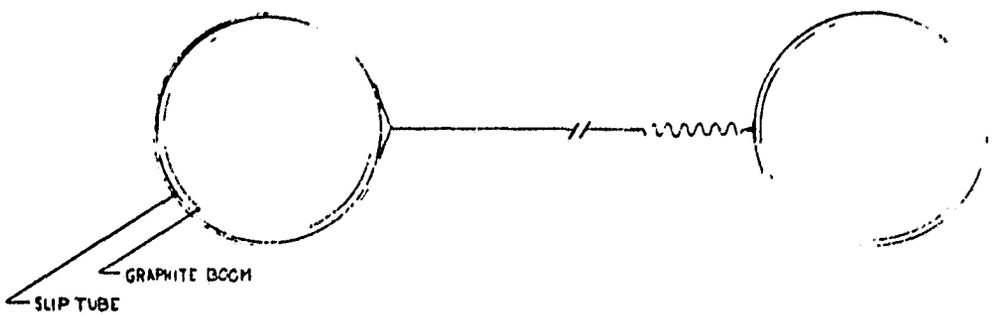

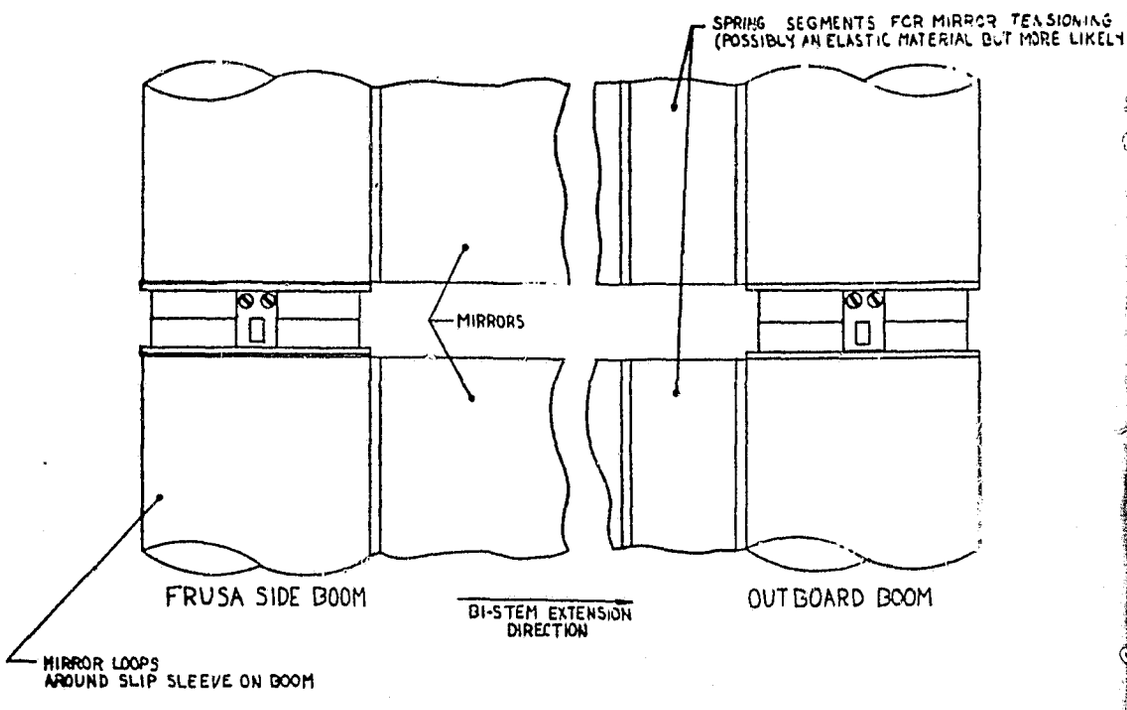

FOLDOUT FRAME

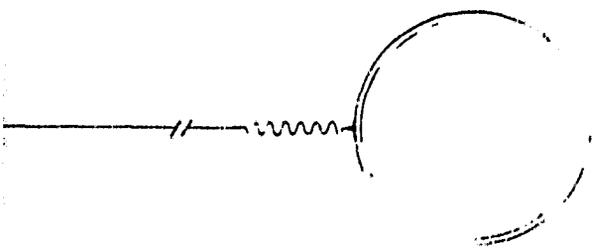

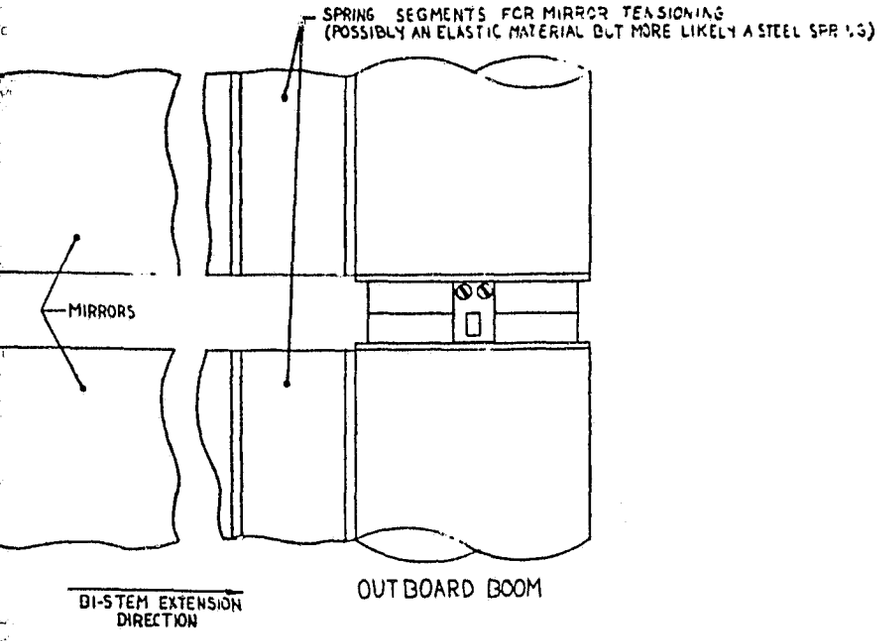

FOLDOUT FRAME 2

QTY REQD	FSCM NO	PART NO OR IDENTIFYING NO	NOMENCLATURE OR DESCRIPTION			ZONE	ITEM OR FIND NO
			PARTS LIST				

UNLESS OTHERWISE SPECIFIED DIMENSIONS ARE IN INCHES AND PER ANSI Y14.5
.XXX ±.010 .XX ±.03 ANGLES ±0°30'
MATERIAL

CONTRACT
DR B. J. Norsc DATE
CHK
APPD

HUGHES — HUGHES AIRCRAFT COMPANY CULVER CITY CALIFORNIA

MIRROR TENSIONING SCHEME
SOLAR CONCENTRATOR STUDY

SIZE E | FSCM NO 82577 | DWG NO 4
SCALE | SHEET

NEXT ASSY | USED ON
APPLICATION